UNIVERSITY
OF TURKU

Fabrication and modeling distributed Bragg reflectors

Department of Materials Engineering, Faculty of Technology
University of Turku
Master of Science in Technology Thesis

Author:
Oskar Tuomi

Supervisors:
Prof. Konstantinos Daskalakis (University of Turku)
Dr. Manish Kumar (University of Turku)

March 2025

The originality of this thesis has been checked in accordance with the University of Turku quality assurance system using the Turnitin Originality Check service.

Master of Science in Technology Thesis
Department of Materials Engineering, Faculty of Technology
University of Turku

Programme: Master’s Degree Programme in Materials of Energy Technology
Author: Oskar Tuomi
Title: Fabrication and modeling distributed Bragg reflectors
Number of pages: 56 pages, 4 appendix pages
Date: March 2025

Distributed Bragg reflectors (DBRs) are dielectric mirrors composed of alternating high and low refractive index materials, which use interference effects from partial reflections within the stack to reflect a tunable range of wavelengths. This property makes DBRs valuable in photonic applications such as lasers, telecommunications, optical filters, and photovoltaics. To achieve a high and uniform reflection band, DBRs require high-quality films, traditionally fabricated using time- and energy-intensive physical vapor deposition methods such as sputtering. Typically, achieving near-100% reflectivity in DBRs requires increasing the number of layer pairs, often exceeding 10 pairs, which in turn demands greater fabrication resources.

In this thesis the main sputtering parameters affecting deposition time for Silicon dioxide (SiO_2) and Tantalum pentoxide (Ta_2O_5) are identified and optimized for DBR purposes. The process of designing and modeling DBRs with established software (WVASE®) is introduced and a novel MATLAB code is developed for simulating the reflectivity spectrums of DBRs. The MATLAB code is intended to be more concise and easier to understand compared to existing codes by focusing purely on the reflectivity modeling by utilizing Fresnel coefficients in a transfer matrix formalism.

The acquired optimized deposition parameters are presented along with the MATLAB code. Resulting reflectivity spectrums from established WVASE® modeling software, the MATLAB code and measured samples are compared, and it is found that the built MATLAB code matches closely. An optimal stack configuration for DBRs is also reported, which achieves close to 100% peak reflectivity with under seven-layer pairs. Notably, a 175% increase in the sputtering rate of Ta_2O_5 is also reported.

Keywords: Thin film optics, Distributed Bragg reflectors, Sputtering, Transfer Matrix Method, Photonics

Table of contents

1 Introduction 1

2 Theoretical background 3

2.1 Thin film optics 3

2.1.1 Polarization 4

2.1.2 Reflection 5

2.1.3 Transmission 7

2.1.4 Absorption 9

2.1.5 Interference 10

2.2 Distributed Bragg reflectors 11

2.2.1 Basic principles of DBRs 12

2.2.2 Applications of DBRs 19

2.3 Transfer matrix method 20

2.4 Thin film deposition 21

2.4.1 Sputtering 22

3 Experimental 24

3.1 Equipment 24

3.1.1 Substrate preparation 26

3.2 Single film deposition 27

3.3 Ellipsometry measurements 29

3.3.1 Determining film thicknesses 29

3.3.2 Acquiring optical constants 30

3.4 Designing distributed Bragg reflectors 32

3.4.1 Modeling DBRs with WVASE software 33

4 Transfer matrix method in MATLAB 36

4.1 Procedure to implement DBR modeling in MATLAB 36

4.2 TMM function 37

5 Results & Discussion 40

5.1 Optimization of deposition time 40

5.1.1 Sputtering power 40

5.1.2 Process pressure 41

5.1.3 Gas flows 43

5.2 Refractive indices 44

5.3 Reflectivity of deposited distributed Bragg reflectors 46

6 Conclusions 52

References 53

Appendices 57

Appendix 1 DBR Code 57

Appendix 2 Transfer Matrix Method Function 58

1 Introduction

Light is a fundamental building block of our world and universe. It gives us vision to observe our surroundings as well as the very energy that forms us. For centuries scientists have experimented and debated about the nature of light and as a civilization we have come to a point where we do not only use light but we can also control it and apply it to multiple different applications. In the field of photonics, control and manipulation of light is used in lasers, light emitting diodes and optical filters. These components form the basis of modern telecommunications. This thesis focuses on one of the components that can be used to manipulate light: Distributed Bragg Reflectors (DBRs). DBRs are 1D photonic structures that can achieve close to full reflection of light on a precisely controlled range in the wavelength spectrum called the photonic stopband. DBR stacks consist of two alternating material layers with low and high refractive indices. With physical vapor deposition methods, it is possible to achieve up to 99% reflectivities on the so-called photonic stopband with as few as 6-layer pairs forming the DBR stack. On both sides of this photonic stopband in the reflectivity spectrum are valleys of high transmissivity called Bragg modes. These unique optical properties make DBRs useful in many applications such as vertical cavity surface emitting lasers (VCSEL), optical fibers, telecommunications and photovoltaics.[1,2]

DBRs can be used to create microcavities by trapping light inside two mirrors. This can in-turn be used to enhance the light-matter interactions to optimize efficiencies of emitting materials and improve the lasing thresholds of laser diodes.[3] What makes DBRs such fascinating components is their simplicity. They only contain two alternating different materials and their optical response, the reflection spectrum, can easily be tuned by varying the layer thicknesses.[1,4]

The goal of this thesis was to optimize sputtering parameters to make depositions of thin films as fast as possible without compromising the quality of the resulting films as well as develop a fast-to-use, simple to understand and easy-to-read MATLAB code to model the reflectivity spectrums of DBRs. The materials used were silicon dioxide (SiO_2) and tantalum pentoxide (Ta_2O_5). First a theoretical background to the physics of thin film optics is presented, followed by the basics of DBRs and their fabrication with a focus on sputtering, which was the deposition method used to fabricate the films in this project. The WVASE software[5] from J.A. Woollam company is presented as a tool that was used in film characterization via ellipsometry measurements as well as modeling and designing the DBRs. The developed MATLAB code is

also presented and results are compared to WVASE modeling and the fabricated DBRs deposited with optimized parameters.

2 Theoretical background

In this section the fundamentals of light propagation are presented in terms of building an understanding on the functionality of DBRs.

2.1 Thin film optics

To understand the function of a DBR, it is crucial to first discuss the basics of light propagation in a material. Light travels through a vacuum or a medium as energy in the form of photons, propagating as an electromagnetic wave. The key factors in a light beam's propagation are the medium it travels through and the interfaces between different media it encounters. When light comes across an interface between two different media, several phenomena can take place, such as reflection, refraction, and transmission.[6–9] These interactions are governed by the principles of wave optics and are essential for designing and understanding thin film structures like Bragg reflectors. In essence, light, as a wave oscillation, interacts with particles at the atomic or molecular level. The concept of "contact" is abstract in this context, as light does not physically touch particles but rather interacts with them through electromagnetic fields. This interaction is happening on a microscopical quantum level and the magnitude of this interaction results in an optical property called refractive index. This gives rise to three major macroscopical effects that are[6–9]:

1) Reflection: Light bounces back from a surface.
2) Transmission: Light passes through an interface and propagates through a material.
3) Absorption: Light gets absorbed by the material in a process where photons excite electrons into higher energy bands.

All of these are affected by the material but also by the properties of light itself. Light is a form of energy, and the amount of energy that the photons forming a beam of light have, determines the frequency of the light wave. This frequency can resonate with atoms and molecules causing a material to show a response. This affects absorption and transmission as well as what happens in the material while and after these effects are happening. Reflectivity is also affected by the angle of incidence, the angle at which light hits the interface between two different media.[3,6]

In thin film optics, the goal is to understand how different materials affect light. This can be done by observing the various phenomena that occur. Reflection of light happens when some

portion of the light's intensity is reflected back from a surface and it is an important property for example in antireflective coatings. The portion of light that is not reflected will travel into the material through the interface and propagate through the material. In thin films, it is important to control transmission to be able to design components such as filters and optical sensors. Not all light will be reflected or transmitted and what is left of the original incident intensity is called absorption. This is the portion of light that is absorbed by the material which it is propagating through. This happens when the energy of a photon is high enough to excite an electron into a higher energy band. Often, this is undesirable because it means the light is lost. However, in some cases, such as in photodetectors, this is the primary goal.

When light interacts with different media, its behaviour is not only influenced by its wavelength and angle of incidence but also by a property called polarization. Polarization refers to the orientation of the oscillating electric and magnetic fields in a light wave. Typically, we describe light as either unpolarized or polarized. Unpolarized light consists of waves with electric fields oriented in random directions, while polarized light has its electric field oscillations oriented in a specific direction.[2,5,6]

2.1.1 Polarization

Polarization refers to the orientation of a light wave's electric field oscillations relative to its direction of propagation. In the context of light reflection and transmission at an interface, two specific polarization states are commonly considered: s-polarization (transverse electric, TE), where the electric field oscillates perpendicular to the plane of incidence, and p-polarization (transverse magnetic, TM), where it oscillates within the plane of incidence. Polarization plays a crucial role in thin film optics, influencing reflectivity and transmission at interfaces. Light can be linearly, circularly, or elliptically polarized, with linear polarization being most relevant in practical applications. Elliptical polarization, for example, is utilized in ellipsometry measurements, which will be discussed in Section 3.3.[5–7] S- and p-polarizations are illustrated in Figure 1 below:

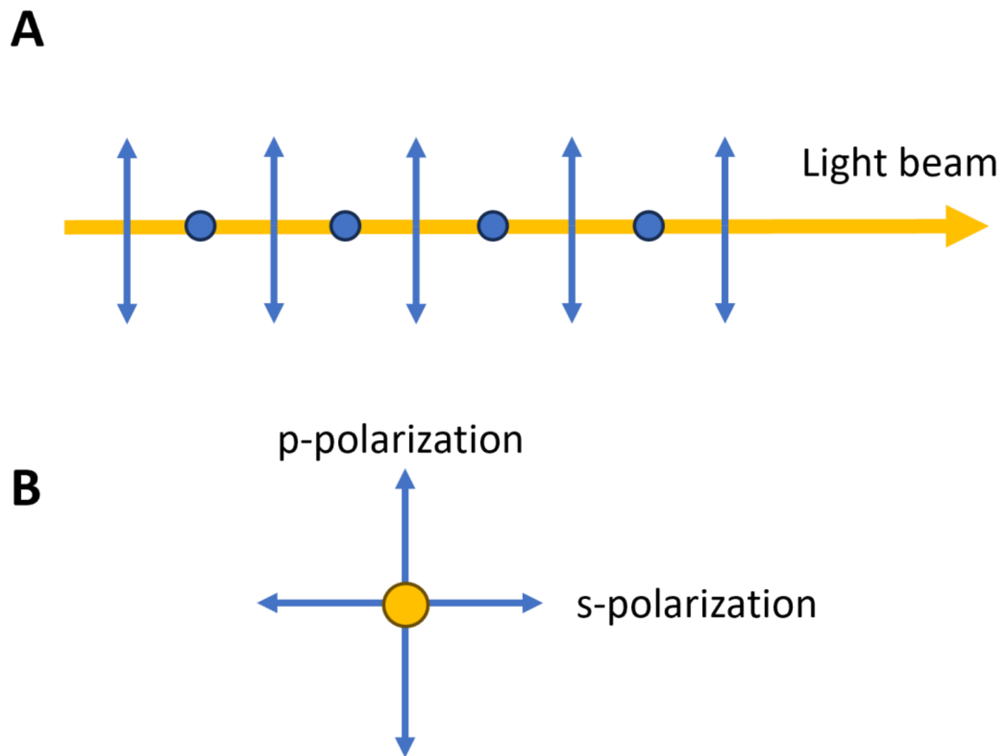

Figure 1: A) Light beam is travelling to the right in the plane of incidence and p-polarization oscillates up and down whereas s-polarization is represented by the dots oscillating in and out of the page. B) Light beam is travelling out of the page and is perpendicular to the plane of incidence.

2.1.2 Reflection

When a light beam arrives at an interface between two different media, it encounters a discontinuity in the arrangement of the atomic structure of the medium it travels in. This discontinuity causes some of the light to be reflected into the original medium. The amount of reflection depends on several factors, such as the incident angle of the light and the refractive index contrast between the two media. The Fresnel equations provide a way to calculate the reflection and transmission coefficients, giving us a quantitative measure of how much light is reflected or transmitted at an interface. At normal incidence (where the light beam strikes the interface perpendicularly), the reflection coefficient r is given by the Fresnel equation:[2,3,6]

$$r = \frac{n_1 - n_2}{n_1 + n_2} \tag{1}$$

where n_1 and n_2 are the refractive indices of the original and new media, respectively. The refractive index of a material is a description of how much the material slows down the speed of light compared to vacuum:

$$n = \frac{v}{c} \tag{2}$$

where *v* and *c* are the speeds of light in the material and vacuum, respectively. The equation from Fresnel also shows that the reflection is higher when there is a greater difference between the refractive indices of the two media. At a normal incidence there is also no difference between the two polarizations resulting in a simpler equation. To get the reflectance one has to take the amplitude of the coefficient[2,3,6]:

$$R = r^2 = \left(\frac{n_1 - n_2}{n_1 + n_2}\right)^2 \tag{3}$$

When light strikes the interface at an angle, the reflection coefficients now depend on the polarization of the incident light. There are two cases to consider: s-polarized (perpendicular) light and p-polarized (parallel) light:

$$R_s = |r_s|^2 = \left(\left|\frac{n_1 cos\theta_i - n_2 cos\theta_t}{n_1 cos\theta_i + n_2 cos\theta_t}\right|\right)^2 \tag{4}$$

$$R_p = \left|r_p\right|^2 = \left(\left|\frac{n_1 cos\theta_t - n_2 cos\theta_i}{n_1 cos\theta_t + n_2 cos\theta_i}\right|\right)^2 \tag{5}$$

where the subscripts *i* and *t* refer to the incident and transmitted angles, respectively. The angle of the reflected light is the same as the incident angle. This is known as the law of reflection[3,6]:

$$\theta_i = \theta_r \tag{6}$$

For p-polarized light, there is a specific angle of incidence at which the reflection coefficient becomes zero i.e. no p-polarized light is reflected. This special case is known as the Brewster angle[5,6]:

$$\theta_B = \tan^{-1}\left(\frac{n_2}{n_1}\right) \tag{7}$$

This property can be used in applications to filter polarization and it can be seen in effect when measuring the reflectivity of distributed Bragg reflectors at increasing angles.

2.1.3 Transmission

When coming into contact with an interface at an angle, the transmitted portion of a light beam experiences bending compared to the normal of the surface on the other side of the interface. This is called refraction and can be described by Snell's law that links the incident and transmitted angles[6,8]:

$$n_1 \sin\theta_i = n_2 \sin\theta_r \tag{8}$$

When light enters an optically denser material, higher refractive index, it bends towards the normal, and in less dense materials, it bends away from the normal. Snell's law can also be used to derive the Brewster angle. The transmitted and reflected beams form a 90-degree angle:

$$\theta_i + \theta_r = 90^0 \tag{9}$$

and with the Brewster angle, where no light is reflected:

$$n_1 \sin\theta_B = n_2 \sin(90^0 - \theta_B) = n_2 \cos\theta_B$$

Solving for θ_B gives:

$$\theta_B = \tan^{-1}\left(\frac{n_2}{n_1}\right)$$

As light travels through a densely packed medium, such as the materials used in DBRs like SiO_2 (silicon dioxide) or Ta_2O_5 (tantalum pentoxide), it interacts with the atoms and molecules of the medium. These interactions depend on the frequency (energy) of the light, and the resonant frequency at which the atoms can oscillate i.e. show a response to the light. These oscillations create secondary wavefronts that combine with the original wave. Due to interference effects in waves, lateral directions cancel out, leaving only the light that propagates forward which is illustrated in Figure 2. This forward propagating portion of the light is

considered to be transmitted through the material. The speed of this transmitted light is determined by the refractive index of the material.[2,6]

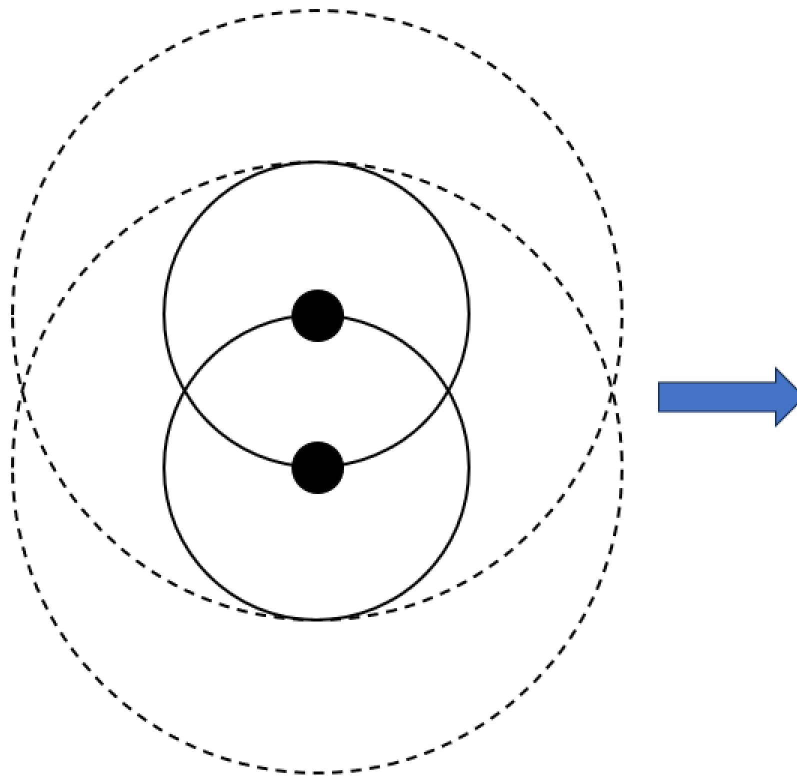

Figure 2: Interference of wavefronts in transmitted light, adapted from Optics by Hecht[6].

According to Snell's Law, light bends towards the normal if $n_2 > n_1$ (where the refractive index of the new medium is higher) and bends away from the normal when it exits the material if $n_2 < n_1$ (where the refractive index of the new medium is lower). This refraction occurs because light takes the path requiring the least time, known as Fermat's Principle. The optical path length (*OPL*) is also an important concept in understanding transmission. It is defined as the product of the refractive index of the medium (n) and the physical path length (s) that light travels through the medium[2,6,7]:

$$OPL = n \cdot s \tag{10}$$

This applies when the medium is isotropic i.e. its refractive index does not vary. In anisotropic cases, the equation for *OPL* can be written as a line integral:

$$\int_A^B n(s)\,ds \tag{11}$$

where A and B represent the starting and end points of the distance travelled, respectively.[3,6–8] The refractive index depends on the material's electronic structure and its interaction with the electromagnetic field of the light wave. Simplified causes for the refractive index are[3,6]:

1. Electronic Polarization: When light interacts with a medium, the electric field of the light wave induces a dipole moment in the atoms or molecules, leading to polarization. The degree of polarization affects the refractive index.
2. Molecular Structure: The arrangement and type of atoms in the material influence how much the light slows down, contributing to the refractive index.
3. Density of the Medium: A denser medium generally has a higher refractive index because the light interacts with more particles as it travels.

Understanding these concepts is crucial for designing and analysing thin film structures like DBRs, where precise control of light transmission and reflection is essential.

2.1.4 Absorption

Absorption of light is a process where photons transfer their energy to an electron in an atom exciting it to a higher energy level. This occurs when the energy of the light is sufficiently high enough to match the transition energies of electrons in the atoms. Considering the function of a DBR stack as a reflector, it is easy to see why absorption is not a wanted property in this case. Losing photons means that the intensity of the radiation drops and it becomes impossible to reach 100% reflectivity. Another issue can arise from the electrons relaxing back to lower energies because while this can happen as an emission of a photon, there are also relaxation mechanisms where the energy transfers to heat or vibrational energy inside the material. Because DBRs are components meant to utilize the reflection phenomena, absorption is detrimental to their function because it decreases the intensity that can be reflected from the maximum theoretical value of 100%. Even if some of the absorbed light will be re-emitted as photons as the electrons relax, it is unlikely that these would be coherent to the main light beam anymore and thus disrupt the partial reflections inside the stack.[3,6,7,10]

At the microscopic level, absorption can be quantified with the absorption coefficient α, similar to the reflection coefficients. According to Beer-Lamberts law the intensity of light propagating in a material decays as a function of the distance x it travels:

$$I(x) = I_0 e^{-\alpha x} \tag{12}$$

where I_0 is the initial intensity. In full accuracy the Beer-Lambert law (12) refers to absorbance which accounts for the attenuation, i.e. the diminishing of the lights intensity, as it propagates through a material. When designing DBRs or other optical components where absorption is unwanted, it is vital to select dielectric materials with minimal absorption in the operating wavelength range.

2.1.5 Interference

In addition to the fundamental properties of light interaction with media, there is also interaction between different light beams themselves. As light is a form of energy this is analogous to waves in the ocean, for example. One of the most famous scientific discoveries was the wave-particle dualism of light. For a long time, there was a debate about the nature of light until the famous dual-slit experiment proved that light acts as particles and waves depending on the situation. This would later form one of the foundations of quantum physics. Interference happens when two or more light waves overlap in space and they combine in that point. Interference can be destructive or constructive depending on the phase differences of the light waves in question. This leads to a concept of superposition of the waves analogous to waves in the ocean. The amplitudes of the waves add together in that space. If the phases match the interference is constructive and the resulting amplitude of the superposition is higher than either individual amplitude. Vice versa, if the phases are opposite, the light waves cancel each other out. In a situation where the phases are exactly the opposite of each other in two waves with similar energies, it appears that there is no light in that instance. This phenomenon is called destructive interference. Interference effects form the vary basis of components like Bragg reflectors.[1,6,7,11]

2.2 Distributed Bragg reflectors

Distributed Bragg reflectors, DBRs, are thin film structures consisting of alternating layers of high and low refractive index materials. When a beam of light travels into this kind of stack of films, it experiences partial reflections at every interface between the two different materials. Engineering correct film thicknesses that affect the optical path lengths of the light beam in the materials allows phase differences to occur, that results in total reflection of certain wavelengths. This phenomenon can be utilized in various applications where the enhancement of reflectivity is desired, such as lasers, telecommunications and anti-reflective coatings.[1,2]

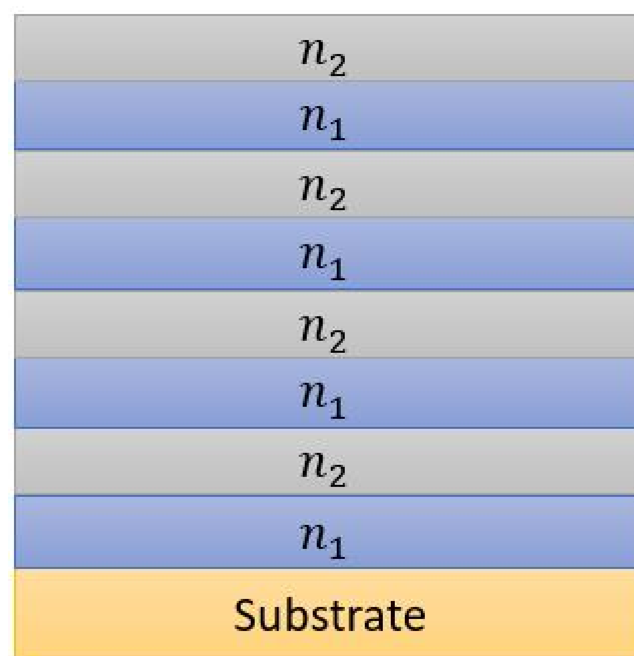

Figure 3: Structure of a 4-pair DBR, where n_1 and n_2 are the refractive indices for the two different materials used.

A DBR is a one-dimensional photonic structure, which affects light passing through it by varying the lights properties along one dimension, the direction of the alternating layers. A structure consisting of four layer-pairs is illustrated in Figure 3. To maximize reflection with the fewest possible layer pairs, materials should have the largest possible difference in their refractive indices and minimum absorption in the desired wavelength range. This creates a photonic stopband on the reflectivity spectrum that can be seen as a counterpart to the electronic bandgap in semiconductors. Main properties of a DBR are the intensity of reflected light, which should always aim to be at maximum (100% of the incident light), the location of the photonic stopband and the width of the stopband. [1,2]

2.2.1 Basic principles of DBRs

As mentioned above, with Bragg reflectors the objective is to reflect certain wavelengths. In a functioning DBR, the incident light travelling through the structure experiences reflection at every interface according to the "Law of Reflection (6)" and refraction that can be described with Snell's Law (8). As this happens on multiple interfaces, the partial reflections from every step start to interfere with each other when they exit the stack on the top surface. When the optical path length of light in each layer matches $\frac{\lambda}{4}$ then the phase differences for the wavelengths interfere constructively and that region of the spectrum exhibits high reflectivity, called the photonic stopband.[11] This is illustrated in Figure 4 below:

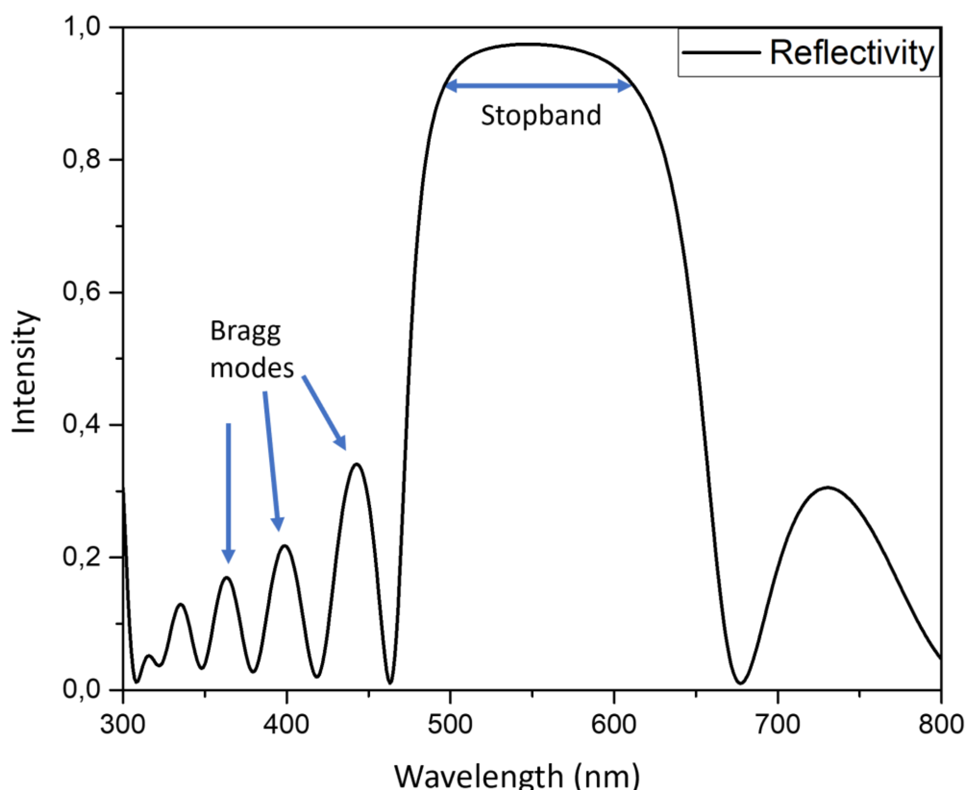

Figure 4: Reflectivity spectrum of a DBR illustrating the photonic stopband and the Bragg modes.

In a reflection spectrum of a DBR, there is the main peak at the desired wavelength and as can be seen from Figure 4 above, there are also smaller, diminishing, peaks in the spectrum on both sides of the main peak, called Bragg modes. These so-called Bragg modes follow Fabry-Perot

interference patterns. The wavelengths at which the peaks are centered on, can be calculated by:[1,12]

$$\lambda = \frac{2}{N}(n_1 d_1 + n_2 d_2) \tag{13}$$

where N is 1,2,3…, with 1 being the peak mode. Taking into consideration also the incidence angle and polarization of the incoming light, the stopband central wavelength can be calculated for s- and p-polarizations, respectively:[1,13]

$$\lambda_s = 4(d_H + d_L)\frac{n_H n_L \cos\theta_H \cos\theta_L}{n_H \cos\theta_H + n_L \cos\theta_L} \tag{14}$$

$$\lambda_p = 4\frac{n_H n_L (d_H cos^2\theta_H + d_L cos^2\theta_L)}{n_H \cos\theta_L + n_L \cos\theta_H} \tag{15}$$

An interesting phenomenon arises when the incident angle differs from zero degrees. Intuitively, this leads to a longer optical path length in the layers, which would cause longer wavelengths to fulfil the quarter wavelength rule and thus lead to a redshift of the spectrum. However, we need to remember that the total reflection consists of partial reflections from all the interfaces experiencing constructive interference. When a reflection travels back from an interface when the incident angle is larger than zero degrees, the reflected rays travelling from different surfaces inside the material experience a phase shift. This causes the wavelengths reflected most at normal incidence to experience less constructive interference because of this phase shift and smaller wavelengths to experience more constructive interference. This actually leads to a blue shift in the spectrum.[1,13]

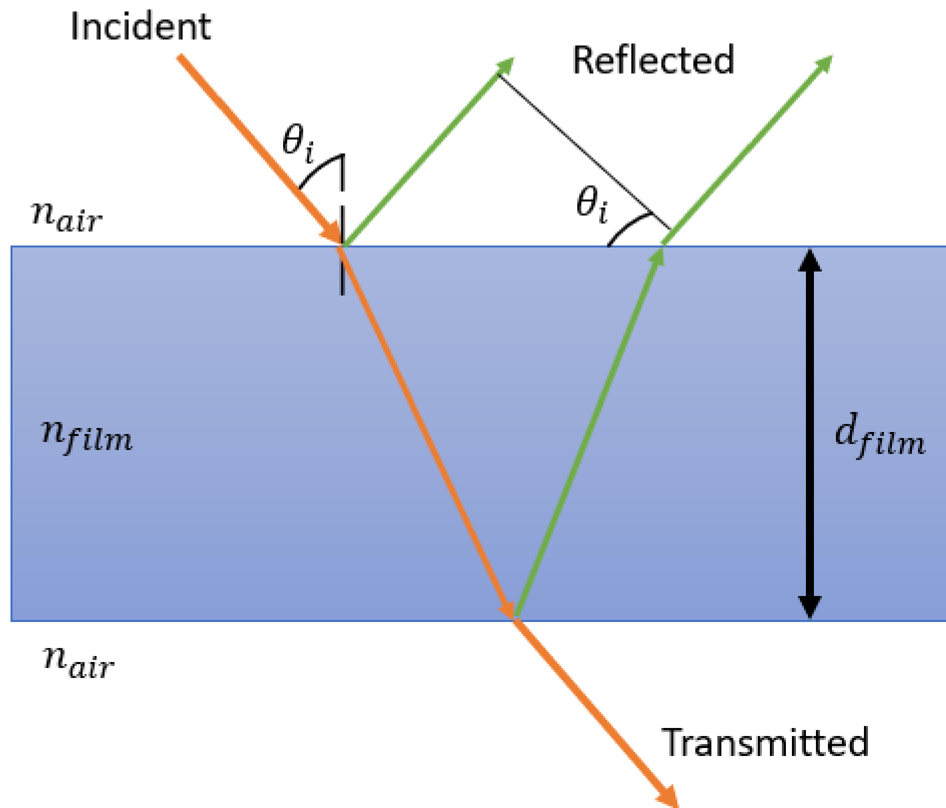

Figure 5: Transmitted and reflected beams of light from a material layer.

The aim is to maximize the peak intensity of the main reflection band. This is achieved when the optical path lengths for each layer correspond to a quarter wavelength of the incident light:

$$OPL = \frac{n_H \cdot d_H}{\cos\theta} = \frac{n_L \cdot d_L}{\cos\theta} = \frac{\lambda}{4} \tag{16}$$

where subscripts H and L denote the high and low index materials, respectively. This equation shows that decreasing either the film thickness or refractive index would lead to a shorter optical path length and thus to a blueshift in the reflection spectrum because shorter wavelengths would now be closer to fulfilling the quarter wavelength rule. The counter-intuitive blueshift of DBR spectrums with higher angles is illustrated in Figure 6.

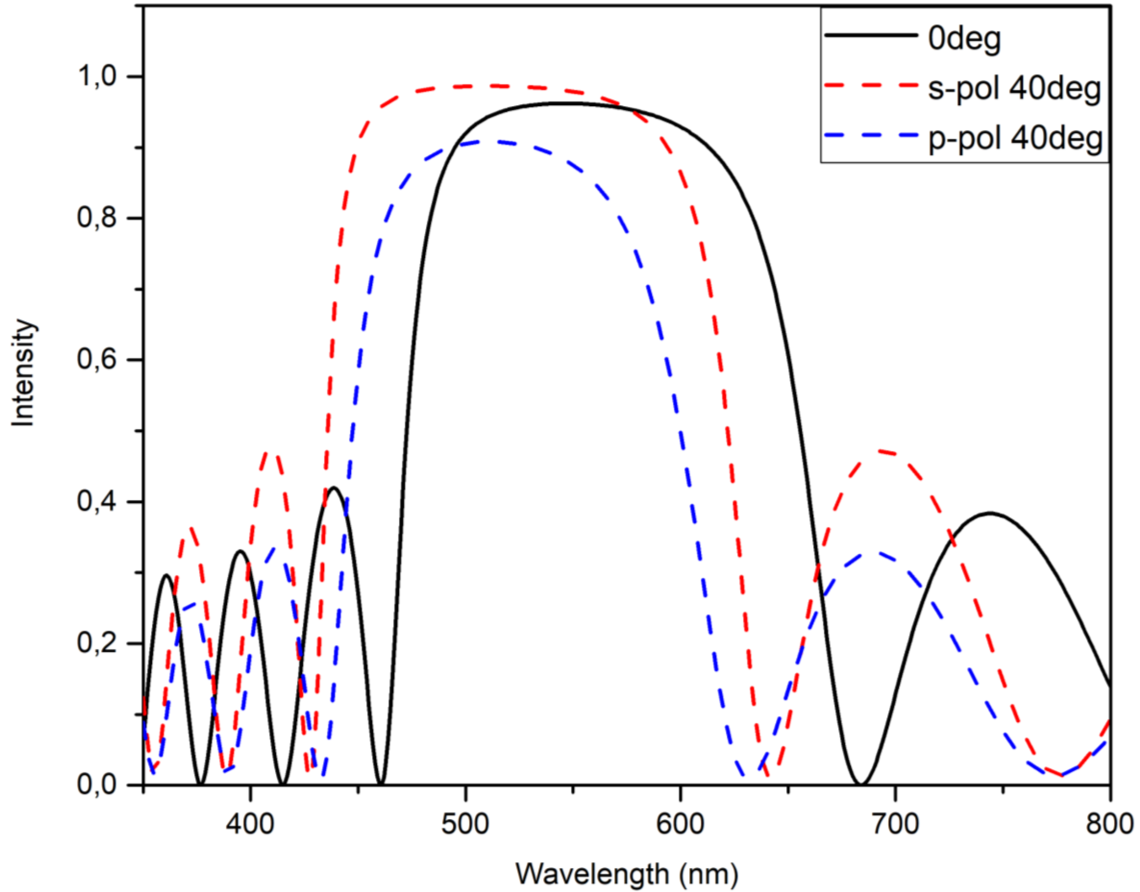

Figure 6: Angle dependency of reflectivity in a DBR for s- and p-polarizations. In both cases, increasing the angle shifts the spectrum to lower wavelengths. In s-polarization, the maximum reflectivity increases where as in p-polarization it decreases.

The theoretical maximum for the reflection intensity is at normal incidence and can be expressed as a function of the number of layer pairs N[14]:

$$R_{max} = \left(\frac{1 - \left(\frac{n_L}{n_H}\right)^{2N}}{1 + \left(\frac{n_L}{n_H}\right)^{2N}} \right)^2 \tag{17}$$

One should note that this equation only holds for an even number of pairs that will be discussed in the results chapter 5.3. This is because it doesn't account for layer order and with 5.5-layer pairs, for example, there are two different configurations depending on which material is deposited as the first layer. This would then also serve as the last layer, meaning there would be a difference in the number of material layers between the two configurations.

The maximum reflectivity is exponentially proportional to the number of layer pairs, so for ideal layers with adequately large contrast in refractive indices the reflectivity reaches 100% fast. For example, for materials that would have refractive indices of 1.45 and 2.15, which roughly correspond to SiO_2 and Ta_2O_5 respectively in the visible range, the peak reflection would follow Figure 7 below:

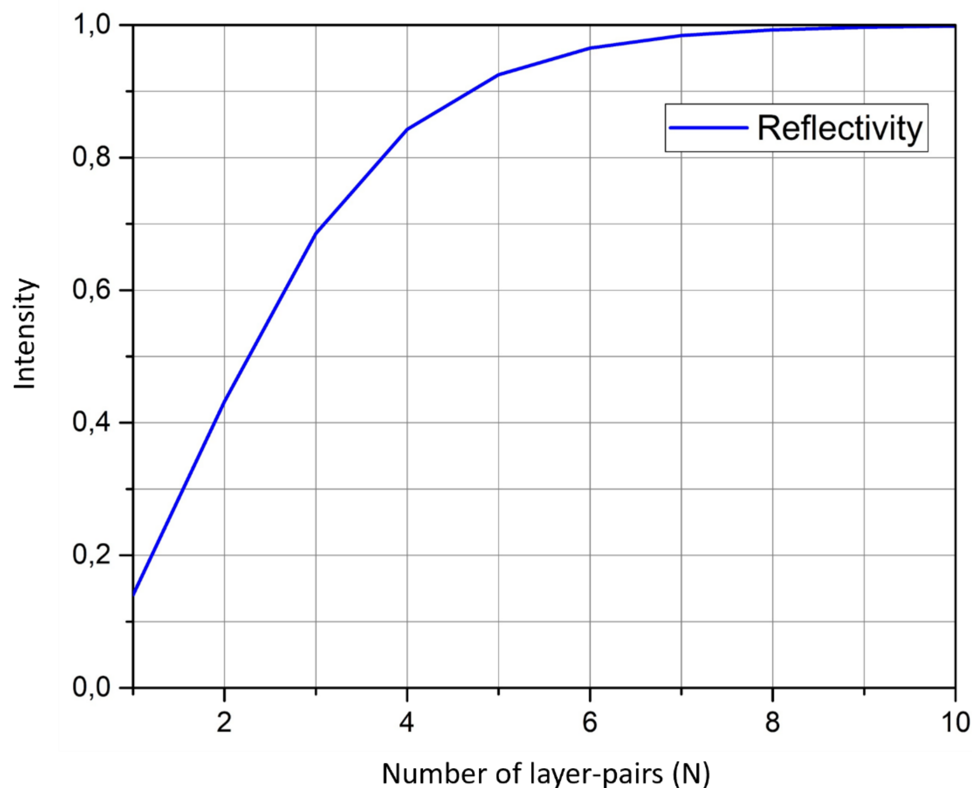

Figure 7: Maximum reflectivity of a DBR as a function of layer-pairs N calculated using equation (17).

It is worth noting that the refractive index is usually dispersive with wavelength so the equation for maximum reflectivity should always be used at a certain wavelength. As Figure 7 shows, the reflectance increases quite rapidly with the used refractive index values as the number of layer pairs N increases. It is pivotal for DBRs to find materials with a large difference in refractive indices, since in reality the increase in layer pairs causes the overall thickness of the structure to grow and thus the number of defects also increases. This leads to a larger deviation from the theoretical maximum. In material selection for DBRs it is also important to use materials with minimal absorption, and even though in the visible wavelength range the chosen materials of SiO_2 and Ta_2O_5 should have next to zero absorption. In reality, there are always

some defect atoms and molecules in the structure that make it difficult to achieve the theoretical values.[1,2] For the layer thicknesses, there can be some deviations from the quarter wavelength rule without too large of an impact on the maximum reflectivity:

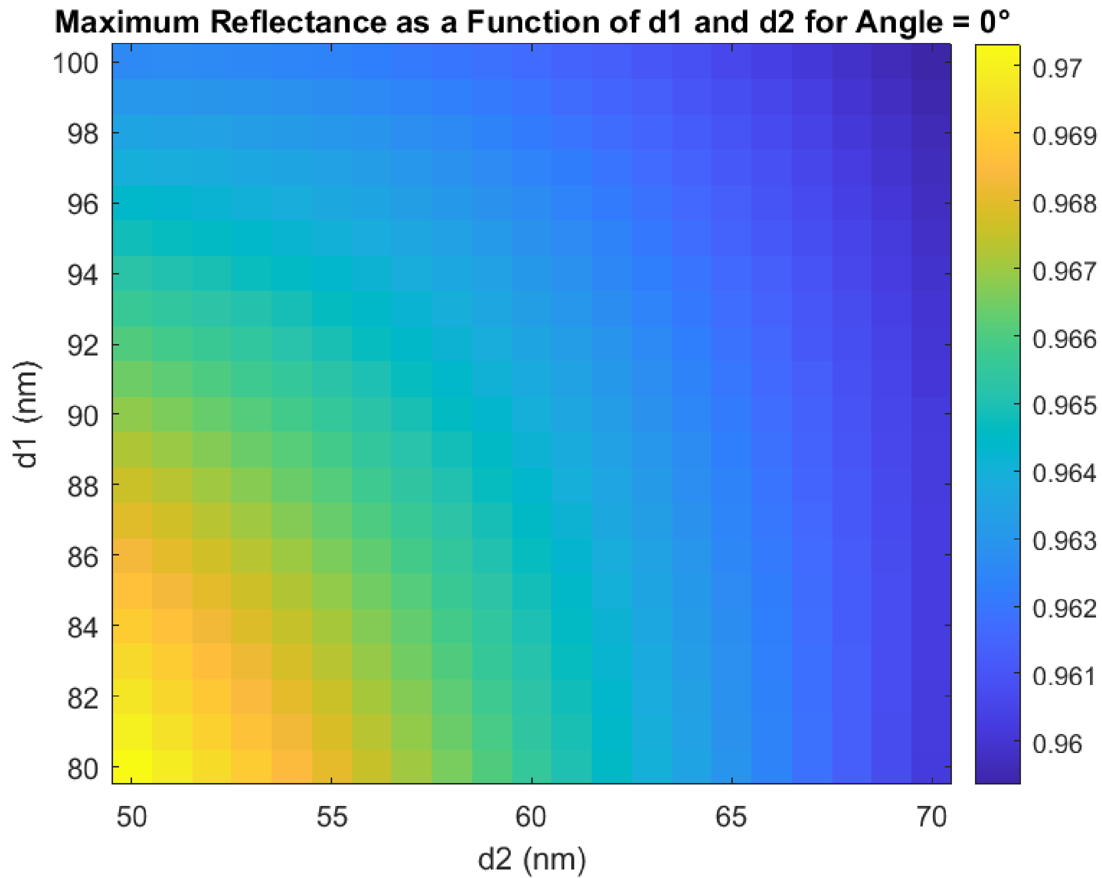

Figure 8: Maximum reflectance of a DBR as a function of layer thicknesses.

Another important property of a DBR is the width of the stopband. Depending on the application, the goal could be to either maximize or minimize the width. Theoretically the maximum width of the stopband at 90% reflectivity is given by:

$$\Delta\lambda = \frac{4\lambda}{\pi}\frac{n_H - n_L}{n_H + n_L} \tag{18}$$

And again, for example with the values 1.45 & 2.15 used earlier for the central wavelength of 550 nm we would get:

$$\Delta\lambda = \frac{4 \cdot 550nm}{\pi} \cdot \frac{2.16829 - 1.47296}{2.16829 + 1.47296} = 133.725 \ldots nm \approx 134\ nm$$

The maximum width of the stopband increases at higher wavelengths. Longer wavelengths are less sensitive to relative deviations in the layer thicknesses and the phases match over a wider range. This can also be illustrated by the connection of wavelength to energy using Planck's equation:

$$E = \frac{hc}{\lambda} \tag{19}$$

where E is the energy of a photon, h is the Planck's constant $6.6261 \cdot 10^{-34}$ J·s and c is the speed of light. This dependency can be plotted:

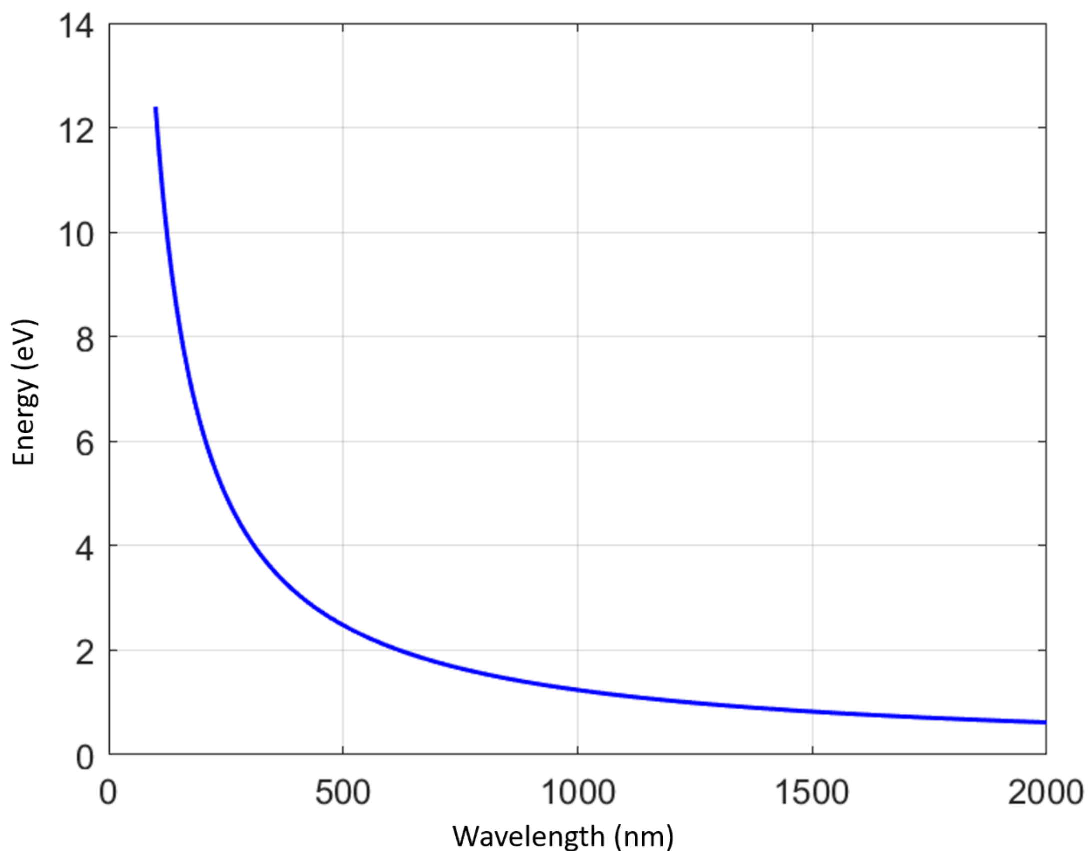

Figure 9: Energy of a photon as a function of wavelength according to Planck's equation (20).

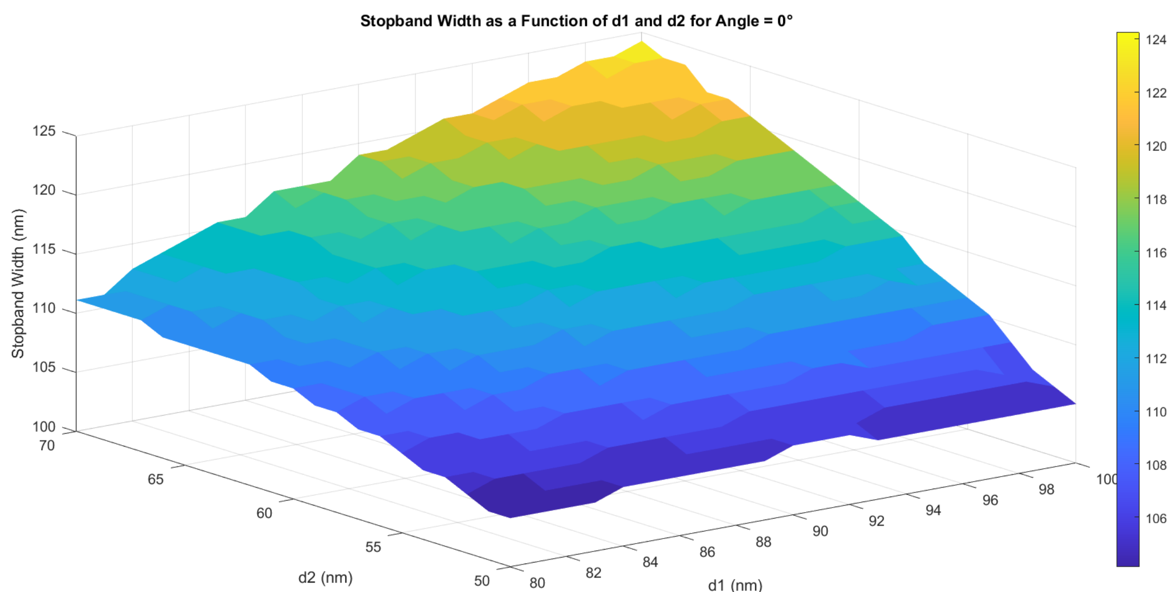

Figure 10: Stopband width of a DBR as a function of layer thicknesses.

The maximum reflectivity for a DBR can be up to 97% with just 5.5 pairs when fabricating them with a physical vapor deposition system. Another interesting property to possibly tune is the width of the stopband. It could be expanded wider by introducing variations in the layer thicknesses. Abe et al.[15] showed that the spectrum can be modified with layer thickness variations without compromising the shape of the stopband. They used a complex machine learning approach with a goal of sharpening the transition into the main stopband and suppress the Bragg modes to the left of the main stopband. This type of approach could also be applied to increasing the width of the stopband by varying the layer thicknesses individually.

2.2.2 Applications of DBRs

DBRs can be used in many applications that require the manipulation of light. Most commercially important application is in vertical-cavity surface emitting lasers (VCSEL), where the light from a laser diode is enhanced between two DBR mirror stacks. This forms an optical cavity where the light is amplified into lasing. The simplicity of the DBRs can be used to tune the output by varying the stopbands of the two stacks. VCSELs are widely used in data communications and they form the basis of optical links in modern data centers.[16,17]

Another interesting application for DBRs is in solar cells. Solar energy has grown rapidly in recent decades and DBRs could help in improving its efficiency in two ways. DBRs could be placed at the back of a solar cell architecture to reflect back light that has transmitted through the active collection layers of the solar cell and, this way return it again to the active layers. This would enhance the light collection capability of the solar panel.[18] Another use case could be to install DBRs in front of the solar cell and tailor them to block UV-radiation that often is harmful for solar panels as it can damage the components and cause wear. Solar cells can only utilize the energy of photons matching their bandgap energies, and any excess energy from lower wavelength photons is turned into heat inside the device. By blocking the higher energy wavelengths, the efficiency and lifetime of solar cells could be improved.[19]

2.3 Transfer matrix method

The basic equations for maximum reflectivity and width of the stopband can offer important information about the main properties of a DBR, however they are not adequate enough to represent the whole reflectivity spectrum, which is an important aspect of a DBR. For this purpose, there exists a powerful mathematical formulation called the transfer matrix method (TMM), which aims to model the response of a thin film stack and its interfaces have on light propagating through the stack. The basic principle of a TMM is quite ingenious in that it represents all the layers and interfaces with characterized matrices where the elements contain information on how the angle and phase of the light changes when its going through the stack. To obtain the total system matrix from which the reflectivity information can be obtained, one simply multiplies all the different matrices together. Existing literature on the subject is quite extensive and all methods utilize boundary conditions on the electric and magnetic fields based on the fact that the interfaces cannot break their continuity, so one can multiply the starting fields at point 0 with the system matrix to obtain the fields at distance d:[1,2,20–22]

$$\begin{pmatrix} E_x(d) \\ H_y(d) \end{pmatrix} = M(k_d, d) \begin{pmatrix} E_x(0) \\ H_y(0) \end{pmatrix} \tag{20}$$

In its simplest form, according to Troparevsky et al[22], the transfer matrix M for a single homogenous layer can be written as:

$$M(k_d, d) = \begin{matrix} \cos(kd) & k^{-1}\sin(kd) \\ -k\sin(kd) & \cos(kd) \end{matrix} \tag{21}$$

where k is the wavevector in the layer with refractive index n:

$$k = \frac{n\omega}{c} \tag{22}$$

The matrix M should always incorporate terms that can represent both the accumulated phase change as the light passes through a layer as well as the diffraction effect that occurs at an interface. As we discuss later on, the terms do not stay quite the same for a multilayer structure with any sort of complexity, but this serves as a building block for the more complicated matrices. For multiple layers one would only construct the transfer matrix M for each layer and multiply them together to obtain the overall system matrix which can be used to obtain the electric and magnetic fields at either end of the system.

$$M_{period,s} = M_{1,s} \cdot M_{2,s} \rightarrow M_{total,s} = {M_{period,s}}^{N} \tag{23}$$

$$S = I_0 \cdot M_{total,s} \cdot I_s \tag{24}$$

where S is the total system matrix and I_0 and I_s are the interface matrices of the first air to material layer and the substrate to air layers respectively. From the final system matrix S, the reflectivity can be obtained by[13,22]:

$$R = \left|\frac{S(2,1)}{S(1,1)}\right|^2 \tag{25}$$

2.4 Thin film deposition

Thin film deposition involves the process of applying a thin layer of a material onto a substrate or on the top of an existing layer. While the basic concept may seem straightforward, achieving a uniform, defect-free film, especially for optical applications, can be challenging. Deposition methods are broadly categorized into vapor-based and solution-based techniques. Physical vapor deposition (PVD) and chemical vapor deposition (CVD), both requiring high vacuum

conditions, offer superior film quality but come at the cost of increased energy consumption and longer processing times. In contrast, solution-based methods like spin and dip coating enable faster, lower-energy deposition but often compromise film quality, particularly when using high-index materials. Among PVD techniques, sputtering is widely used for high-quality optical coatings and will be discussed in more detail in the next chapter.[1,4,23]

2.4.1 Sputtering

Sputtering is a form of physical vapor deposition where a source material is bombarded with plasma ions of a non-reactive gas. These ions hit the source with enough energy to release atoms from the surface of the material and then they get deposited onto a new layer on the substrate[24–26].

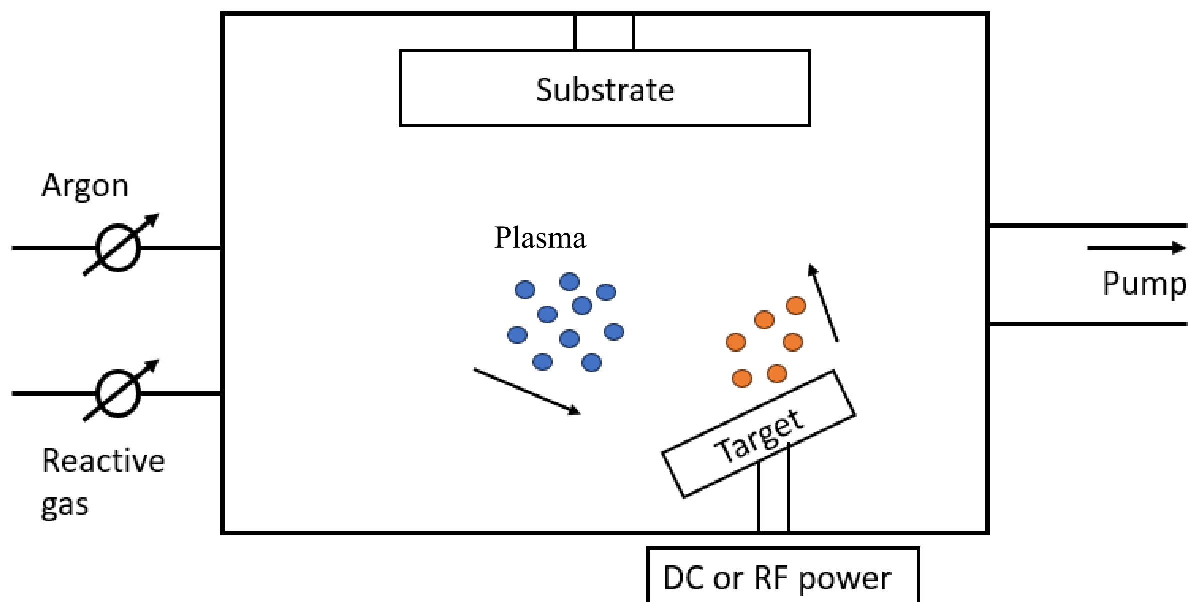

Figure 11: Schematic of a sputtering process, adapted from Berg[24].

In the sputtering process illustrated in Figure 11, argon plasma is created in a vacuum chamber with an electric field that is then used to accelerate the argon ions towards the target material. These ions hit the atoms of the target material with enough energy that the target atoms break free of their bonding and are ejected from the target. The plasma cloud in the vacuum chamber is kept at a low pressure to minimize collisions with the target atoms as they travel towards the substrate, where they condense together again to form the resulting film. Argon is often used as an inert gas because it has sufficient atomic mass resulting in energetic collisions, low

chemical reactivity as a noble gas to prevent further reactions with the target material and relatively low cost compared to other inert gases. In some cases, a reactive gas, such as oxygen, is also inserted into the chamber to combine with the ejected target atoms to form the film. An example of this use case would be the deposition of a Ta_2O_5 film, where oxygen is involved in bonding with the tantalum atoms used as a target material.[24]

The key parameter in sputtering is called the deposition rate, which refers to the rate at which material is deposited onto a substrate, usually represented as ångstroms/second. This is determined by the sputtering yield (number of ejected atoms per incident ion) and the chamber's pressure. More ejected atoms mean more atoms deposited and lower pressures of the process means less collisions on the way to the substrate, leading to faster rates. A minimum pressure level is needed to ignite and maintain the plasma. The sputtering yield depends on the ion's size and energy as well as the bonding energy of the target material. With modern equipment, it is easy to control the energy for the collisions and since higher power is directly proportional to the sputtering yield it is generally as high as the target can withstand. However, longer exposures to higher powers result in faster target deterioration and this is a trade-off one should consider.[24,25]

RF sputtering is a form of sputtering that uses radio-frequency energy, typically at 13.56 MHz, to create plasma and sustain the deposition process.[26] Unlike the more cost-effective DC sputtering, RF sputtering alternates the polarity of the target at a high frequency, which prevents charge build up on the target. This allows continuous ion bombardment and more importantly allows the use of non-conductive targets as well. Another benefit of RF sputtering is the oscillations it causes in the plasma, which helps in keeping it stable at lower pressures. The use of dielectric materials is especially important in optical coatings and semiconductor devices, for example, taking advantage of SiO_2. The drawbacks of RF sputtering come in the form of more complex and expensive equipment and also the deposition rates can be lower for certain materials that also could be sputtered using DC sputtering.[24]

3 Experimental

In this section, all the relevant experimental methods and equipment used will be presented. As the goal of this thesis was to optimize the deposition parameters for distributed Bragg reflectors, there was a starting point to use the existing recipes of the Luminous Materials Devices research group at the University of Turku. The workflow started with depositing single films of SiO_2 and Ta_2O_5 with the existing recipes and then varying the most important parameters identified by literature review. The sputtering targets used were SiO_2 and tantalum, with the Ta sputtering requiring oxygen flow into the chamber along with the Argon gas that was used as the ion source, while for SiO_2, only argon was used. The films were deposited on both quartz and silicon substrates. The evaporator used in sputtering was the EvoVac 720 from Angstrom Engineering. Transparent quartz substrates were used to measure the reflectivity and transmissivity of the films, and silicon substrates were used to acquire refractive index data for the films via spectroscopic scan with a WVASE ellipsometer from the JA. Woollam company. The WVASE software was also used to construct general oscillator models for both materials based on the measured refractive indices. These models were then used both in the WVASE software and MATLAB to design and model DBRs. For MATLAB a simple transfer matrix code was developed to model the reflectivity of the samples and make it easier to design and plan DBRs to be fabricated.

3.1 Equipment

Two main pieces of equipment were used in the experimental works of this project.

A) The sputtering was performed with the Angstrom Engineering EvoVac 720 evaporator. It contains multiple source locations inside a vacuum chamber that are illustrated in the schematic Figure 12 below:

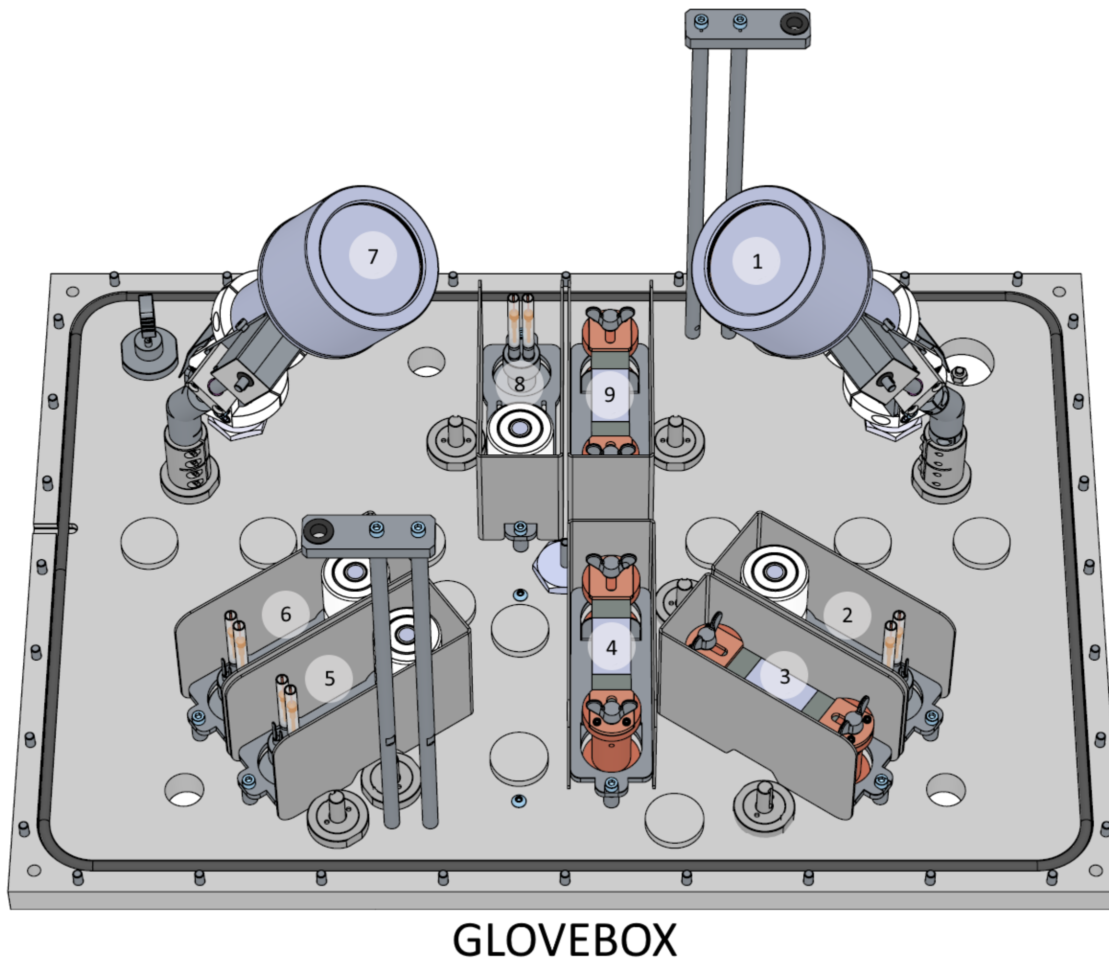

Figure 12: Schematic of the evaporator showing different types of sources, such as resistive sources for metal deposition (3,4,9), high temperature Radak sources for organic materials (2,5,6,8), and 2 RF-sputter guns (1,7).

Sources 1 and 7 contain the sputtering targets, in this case SiO_2 and Ta_2O_5 respectively. In this evaporator the maximum power that can be directed to the plasma and sputtering targets is 600W using an AC power source.

B) Film thicknesses and reflectivity spectrums for fabricated films were acquired through variable angle spectroscopic ellipsometry measurements by performing a spectroscopic scan on the JA. Woollam WVASE ellipsometer presented in Figure 13 below:

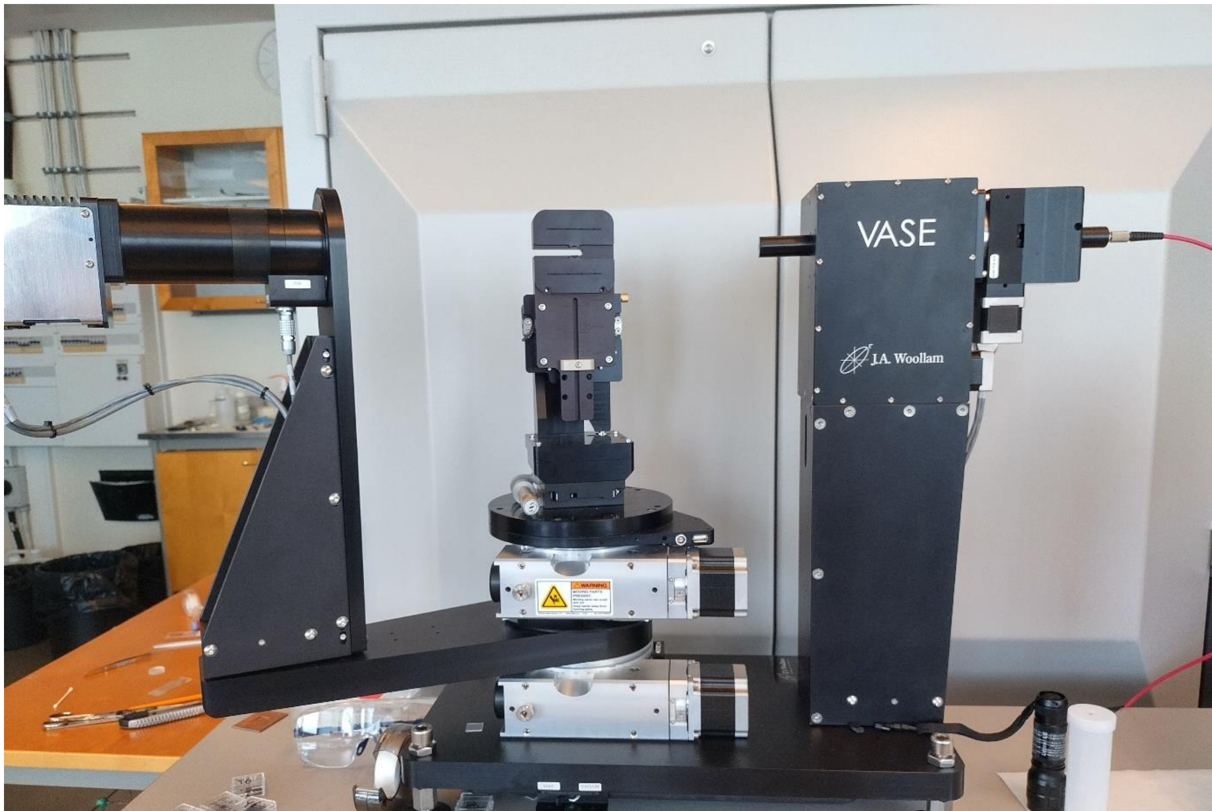

Figure 13: Ellipsometer from JA. Woollam Company.

Ellipsometry is a widely used measurement technique used to characterize thin films. In an ellipsometry measurement light with a known polarization state is irradiated on a sample and then the relative phase changes in the polarization state are measured from the transmitted or reflected beams. The parameters observed during a measurement are the phase difference, delta (Δ), of s- and p-polarized components of the light, and the amplitude ratio, psi (Ψ), between s- and p-polarized light. With ellipsometry measurements, it is possible to determine the thickness of a sample as well as the optical constants *n* and *k*. In the VASE ellipsometer by J.A Woollam that was used in this project, the light is produced by a Xenon lamp.[5]

3.1.1 Substrate preparation

All the depositions in this project were made on two different kinds of substrates: fused silica (Quartz) and silicon (Si). Both types of substrates were 1mm thick and 15x15mm^2 sized squares. The silicon substrates were used for single film depositions to acquire the *n* and *k* data via the ellipsometer while the quartz substrates were used for DBR depositions as well as measuring reflectivity and transmission of single films. Before depositing materials in the evaporator, the substrates were cleaned with a five-step process:

1. Sonication for 10 minutes in distilled water with Decon90 soap.

2. Flush the soap with 80°C hot de-ionized water and then sonicate for 10 minutes in the hot water.
3. Rinse substrates with acetone and sonicate for 10 minutes in acetone.
4. Rinse substrates with IPA and sonicate for 10 minutes in IPA.
5. Blow dry the substrates with high purity N5 nitrogen.

After every sonication the substrates were rinsed with the next steps solution to minimize cross-contamination and after blow drying, the substrates were immediately transferred to a vacuum environment inside a glove box.

3.2 Single film deposition

According to literature, the main sputtering parameters impacting the deposition rate and resulting film quality are the used sputtering power, process pressure and gas flows into the sputtering chamber.[24,27,28] Starting point recipe parameters for the sputtering of SiO_2 and Ta_2O_5 films existing in the research group are presented in Table 1 below. The sputtering power is presented as a percentage of the maximum that can be provided by the source, which in this case is 600 W.

Table 1: Initial sputtering parameters.

	Power [%]	Pressure [mTorr]	Ar Flow [SCCM]	O_2 Flow [SCCM]	Rate [Å/s]	Target thickness [nm]	Measured Thickness [nm]
SiO_2	30	5	15	0	0.33	60	61.3 ± 0.2
Ta_2O_5	45	5	20	10	0.51	60	57.6 ± 0.1

For the first depositions with the parameters specified in Table 1 above, the rates matched the previous depositions done in the host LMD group. The maximum power used in sputtering is determined by the target material and its area. Both of the targets used in this project were the same size (circular discs with a diameter of three inches), but since tantalum is a metal with high electrical and thermal conductivity, the used power could be higher compared to the SiO_2 target. The higher the power the higher the rate, thus leading to a faster deposition. This makes intuitive sense since with higher power the plasma-ions have more energy and are able to separate more target atoms and molecules which then have higher energies after leaving the

substrate. The deposition rate increases linearly with the power used, so it makes sense to use maximum power to achieve the highest possible rate. However, this can damage the sputtering target during longer DBR depositions, because it exposes the target to higher forces and temperatures. During the later DBR depositions the SiO_2 target showed unnecessary levels of wear on its surface and a leaking of the indium bonding between the target and its copper backplate, suggesting insufficient heat transfer.

The other two important parameters, process pressure and gas flows, are intrinsically linked. Lower pressures and higher gas flows require more outflow by the system and vice versa. With these parameters, the effects can be described quite simply on the macroscopic scale. As discussed earlier, in sputtering the purpose is to hit the target material with argon ions separating atoms and then the target atoms deposit onto the substrate. The highest rates are achieved when there are the least non-favourable collisions on the path from the target to the substrate. Thus, the reasoning is to minimize the number of particles in the chamber during deposition i.e. minimizing pressure and gas flows. However, for the plasma to ignite there must be enough argon gas at an adequate pressure. The process pressure and gas flows can have a significant impact on the final thickness and especially its deviation from the target thickness.[24,27] The sputtering time used is calculated by inserting the target thickness as a parameter and then at the start of the process a sensor in the chamber is used to measure the deposition rate. The software uses this measured rate to set the time that is used for sputtering. For the sensor to give accurate readings, the process needs to be stable and there needs to be an adequate number of particles.

To deposit materials onto substrates the process used was the following:

1. Clean substrates and transfer them into the glovebox.
2. Insert the substrates onto a substrate holder that is placed inside the evaporator at the top of the vacuum chamber.
3. Create sputtering recipes and/or sequences if combining multiple recipes.
4. Start the sputtering process.

3.3 Ellipsometry measurements

3.3.1 Determining film thicknesses

To determine the thickness of a thin film and acquire information about its optical constants, a spectroscopic scan is performed on the ellipsometer. In the measurement, the sample is hit with a light beam with desired wavelength resolution throughout a range of 300-1300 nm. This wavelength range is selected because tantalum has absorption below 300 nm and the visible range starts around 350 nm. The ellipsometer measures two parameters: delta (Δ) and psi (Ψ). Delta (Δ) represents the phase difference between the s- and p-polarized components of light after it reflects off the sample, while psi (Ψ) indicates the ratio of the amplitudes of the two polarizations. The measurement is repeated for angles of 55, 65 and 75 degrees, which are selected around the Brewster angle. After measuring experimental data, a model of the sample is constructed in the WVASE software, where a layer of Cauchy material (a layer described by Cauchy dispersion relation) is added above a silicon substrate. This relation is widely used to model the response of a transparent material.[5]

$$n(\lambda) = A + \frac{B}{\lambda^2} + \frac{C}{\lambda^4} \quad (24)$$

where A, B and C are coefficients for a specific material.

Based on this model, the WVASE software can generate theoretical values for the measured properties, which can then be fitted to the experimental data to acquire probable parameters.[5] Fitting the ellipsometry data starts by providing an initial value for the film thickness. A reasonable guess is always the thickness determined as a goal in the deposition and then a normal fit is performed in the transparent range of the data. Figure 14 shows the data for a Ta_2O_5 film deposited in 1 mTorr pressure. From the Ψ data, the transparent region is the flat area of the curve starting from approximately 800 nm. Firstly, a Cauchy fit was performed in the range of 800-1300 nm leading to a thickness value of 59.6 nm and a MSE of 1.46. Then the lower threshold of the range is decreased in steps and new fits are performed while observing the change in thickness and MSE until an adequate result is obtained.

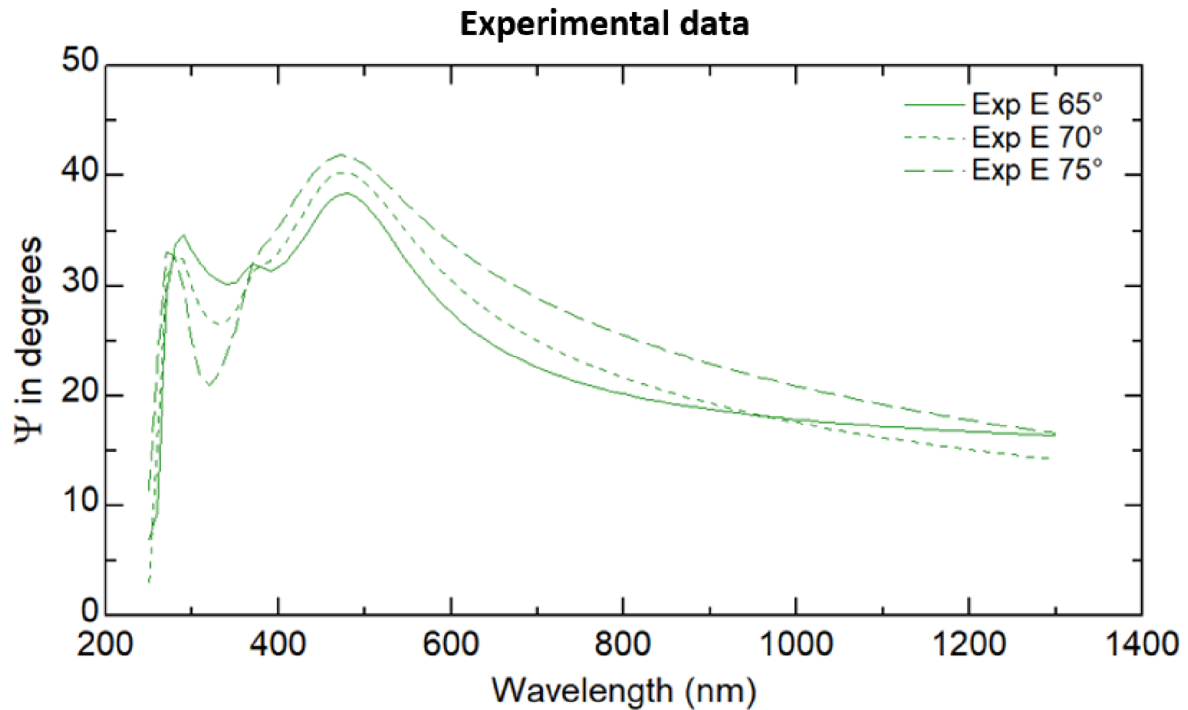

Figure 14: Measured Ψ data from a Ta_2O_5 film deposited on a silicon substrate. During deposition the target thickness was selected as 60 nm, which is used as an initial guess for the thickness in the WVASE software before starting the Cauchy-fitting on the transparent region of the data. This figure was copied from the WVASE software user interface.

3.3.2 Acquiring optical constants

After a value for the film thickness has been identified with WVASE using the Cauchy model in the transparent region, the next step is to acquire refractive index data. This includes also the extinction coefficient *k* which describes absorption. For DBR purposes, we can limit the analysis to the near-UV and visible range of around 300-800 nm. In this range the used materials practically have a *k* value of zero, which is pivotal to the function of a DBR. There are multiple articles[29,30] offering reference data for the refractive indices of SiO_2 and Ta_2O_5 which can be used to cross reference the measured values from in situ deposited thin films. To measure n- and k-values for a thin film with an ellipsometer, the film is deposited on a silicon substrate. The film is then placed on the ellipsometer and a spectroscopic scan is performed. Then a model is constructed using the WVASE software, where a Cauchy-material is inserted above the substrate.

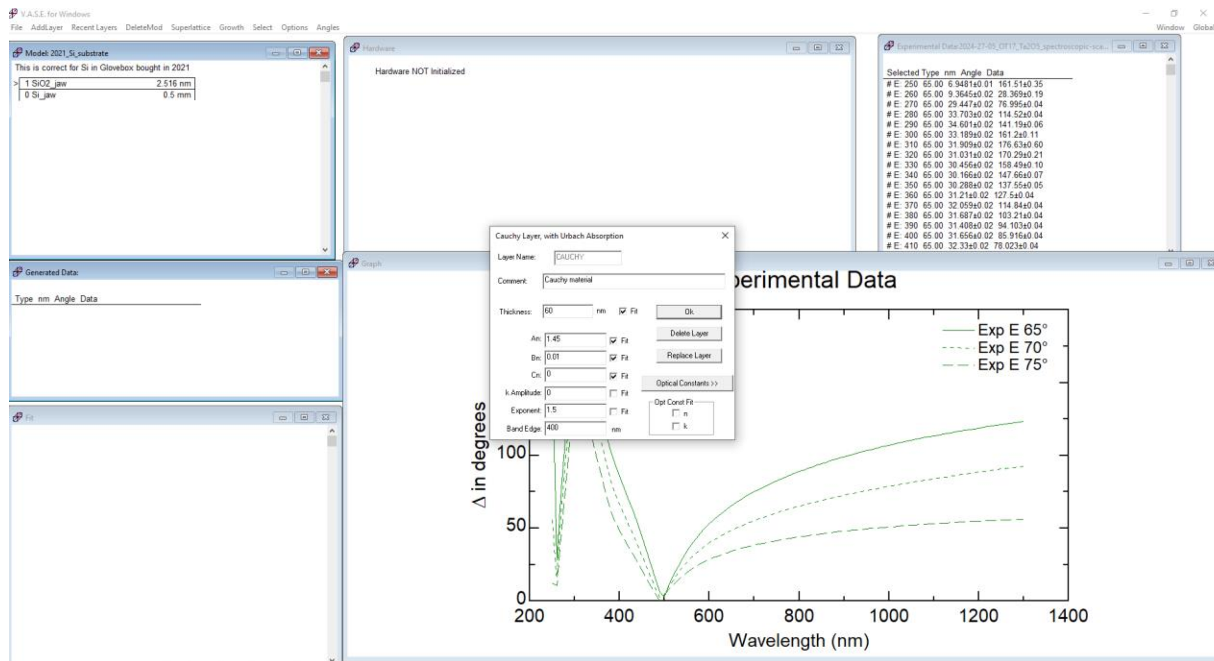

Figure 15: Inserting a Cauchy layer in WVASE software on top of a model of a silicon substrate. The layers will appear in the top left window of the interface. The pop-up window at the center shows the different parameters used in fitting. First, when fitting layer thickness, the thickness, An, Bn and Cn parameters are first chosen. The latter three describe the dispersion of light that the film is causing. After acquiring an adequate value for layer thickness, the earlier parameters are unchosen and the n & k are fitted next.

After performing Cauchy fits to find the thickness of the film, the thickness is removed as a fitting parameter and *n* & *k* values are chosen instead. The fitting range is also increased to the range of the whole measurement and a point-by-point fit is performed. Acquired indices for a fabricated sample using this procedure are depicted in Figure 16:

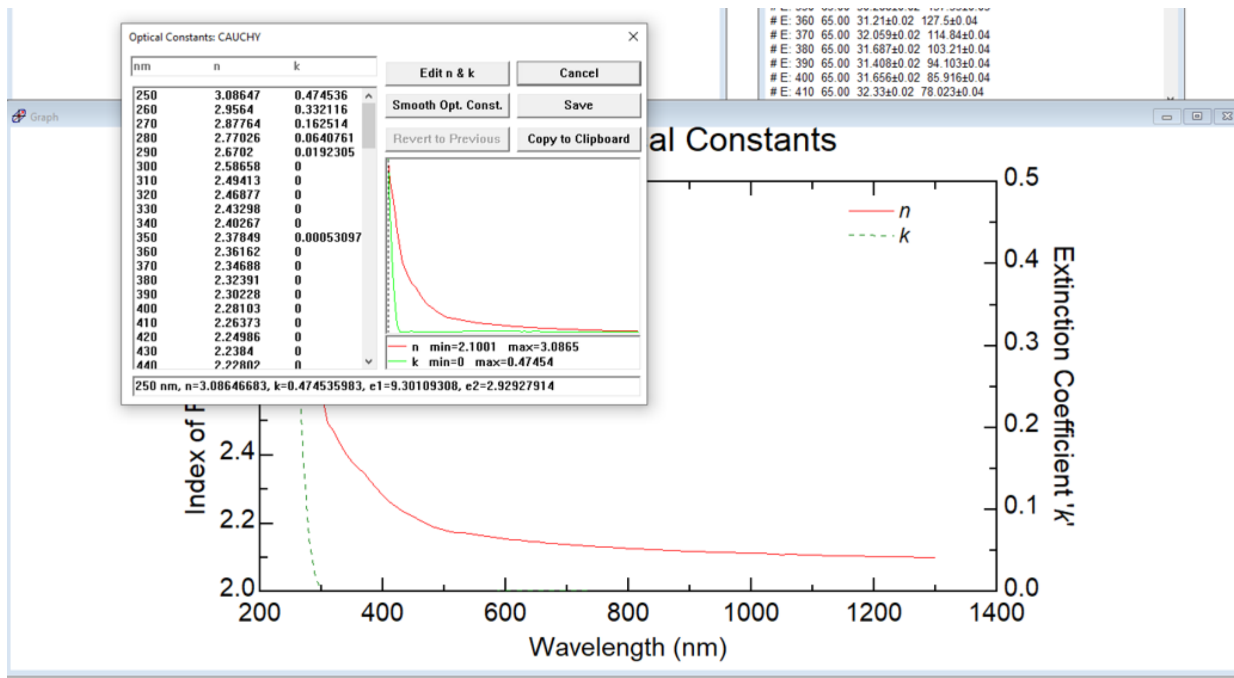

Figure 16: Acquired optical constants in WVASE software after fitting the measured ellipsometric data.

The limitations in these fits come from the very small absorption coefficient k experiencing large noise due to the small nature of the value in the observed range. This can lead to the fits violating the Kramer-Kronig relation. The Cauchy model also does not enforce this relation which can lead to initially unrealistic models. The Kramer-Kronig relation is a set of integral relations that enforce causality and consistency between the real and imaginary parts of the optical constants n and k.[31] To overcome this the WVASE software allows a possibility to build a general oscillator layer from the measured values. This ensures that the measurements follow the laws of physics and are self-consistent. The GenOsc model uses oscillator functions – such as Lorentz, Gaussian and Tauc-Lorentz – to describe the dispersion response to light by the material. These functions are derived from the frequency dependence of the dielectric function and the physical basis of these relations are the molecules and atoms in a material that act as oscillators when affected by the propagation of light.[5,31]

3.4 Designing distributed Bragg reflectors

The primary consideration in designing a DBR is to identify its usage. For example, when utilizing two DBR stacks to envelope an emitting material to create a microcavity, one needs to identify the stopband around the emission wavelength of the emitting material so the emission can be trapped and enhanced. Another criterion to remember from the DBR theory discussed in section 2.2 is that the layer thicknesses should follow the quarter wavelength rule

throughout the stack to maximize the peak reflectance. For SiO_2 and Ta_2O_5 used in this project, the target for the stopband center is selected at 550 nm, which is used for the target layer thicknesses that can be calculated with equation 16:

$$d_{SiO_2} = \frac{\lambda_0}{4 \cdot n_{SiO_2}} = \frac{550\ nm}{4 \cdot 1.473} = 93.35\ nm$$

$$d_{Ta_2O_5} = \frac{\lambda_0}{4 \cdot n_{Ta_2O_5}} = \frac{550\ nm}{4 \cdot 2.168} = 63.42\ nm$$

The theoretical width of the stopband for these materials and thicknesses would be:

$$\Delta\lambda = \frac{4 \cdot 550\ nm}{\pi} \cdot \frac{2.16829 - 1.47296}{2.16829 + 1.47296} = 133.725 \ldots nm \approx 134\ nm$$

This value is typically given at 90% reflectivity value.[13] The maximum reflectivity values for full number of pairs in this DBR structure according to equation 17 are:

Table 2: Number of layer pairs and corresponding maximum reflection.

Number of layer pairs N	R_{max}
2	0.42
3	0.67
4	0.83
5	0.92
6	0.96
7	0.98
8	0.99

3.4.1 Modeling DBRs with WVASE software

Using target thicknesses for the material layers based on theoretical calculations and tabulated values from the built general oscillator models, the DBR stack can be modelled using the WVASE software. The theoretical modeling can be cross-referenced with the WVASE modeling, which can provide a reflectivity spectrum for the DBR stack. In Figure 17 is the

generated p-polarized reflectivity spectrums of a 5.5 pair DBR centered at 550 nm with four different incident angles:

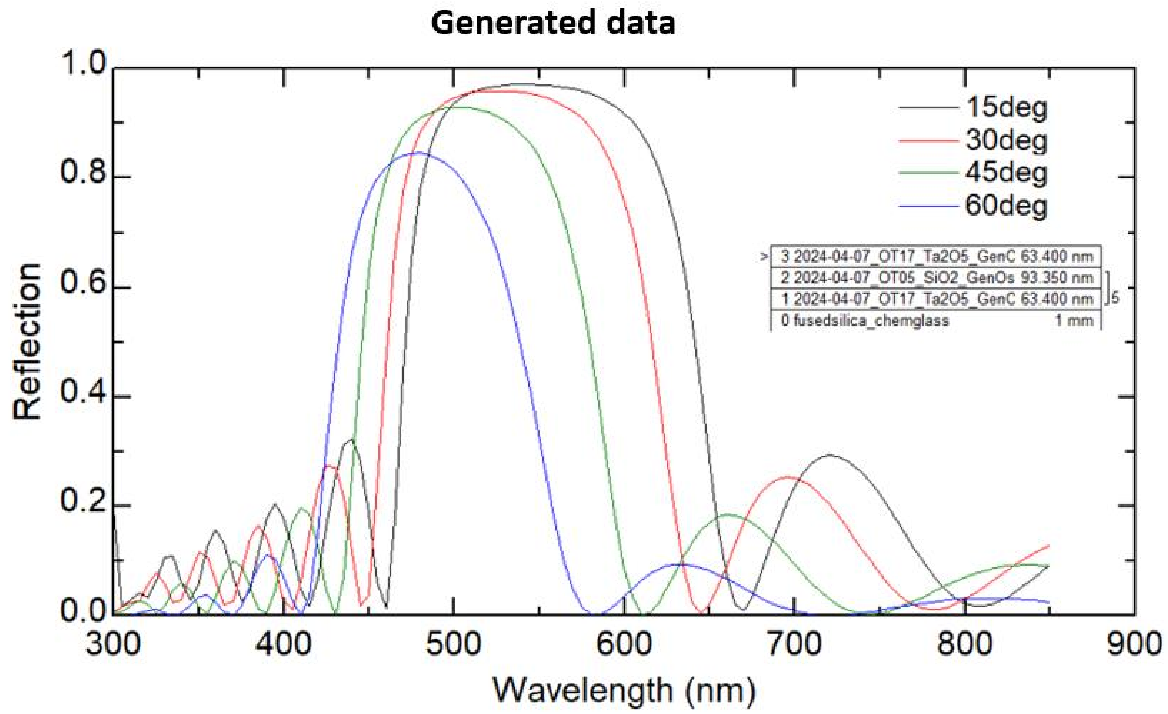

Figure 17: Modeling a DBR reflectivity spectrum in WVASE software for multiple angles. The figure was copied from the WASE user interface.

To model a DBR stack, the built material models (general oscillator layers) are added with layer thicknesses. The software can plot desired properties like reflectivity and transmission for multiple angles as well as different polarizations. A useful design objective is to identify the layer order. In Figure 18 below is plotted the reflectivity spectrums for four different stack configurations, 5.5 pairs and 6 pairs, with changing layer order while keeping the thicknesses same. It can be seen that there is a large discrepancy between the 5.5 pair stacks that can be attributed to the number of the high index Ta_2O_5 layers that reflect more light. It also seems that for maximum reflectivity it would be beneficial to end the stack in the high index material.

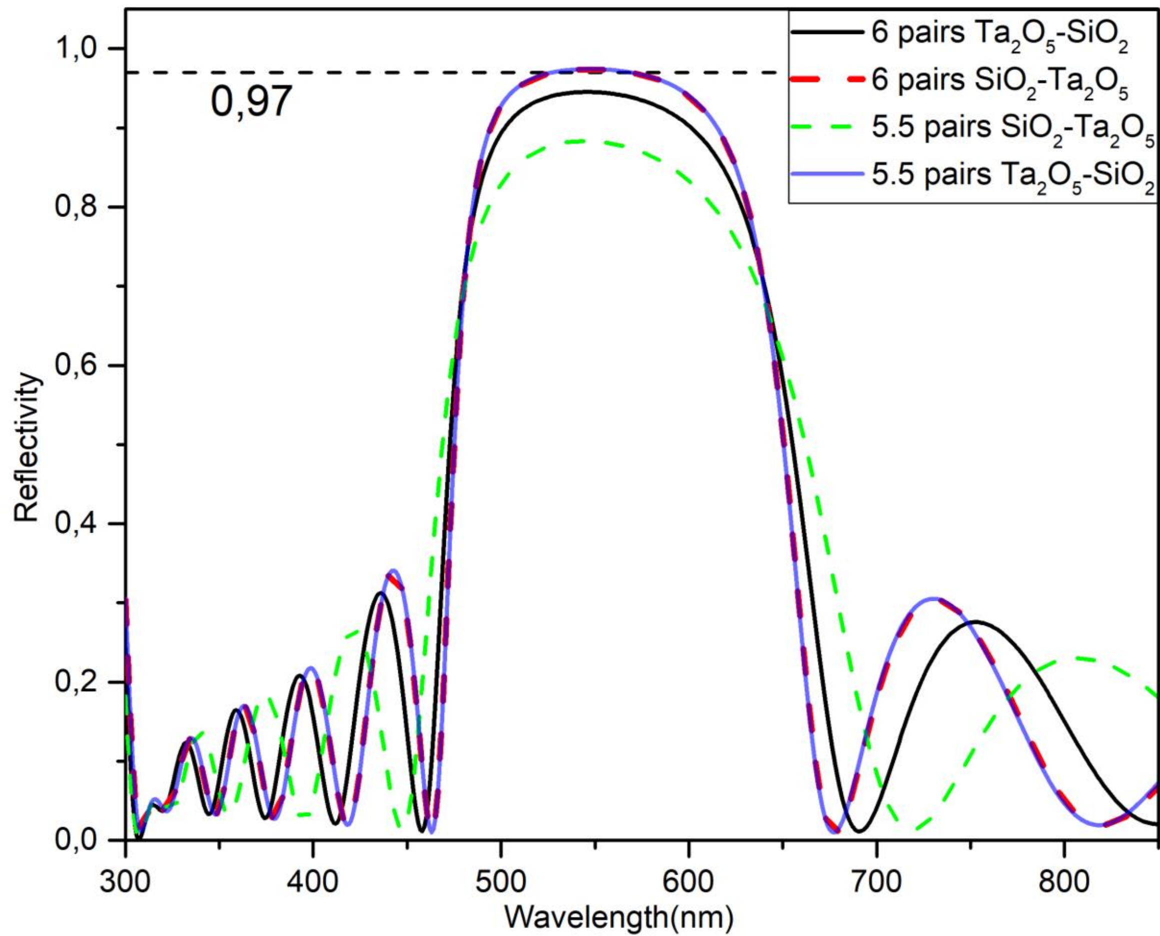

Figure 18: Reflectivity spectrums of four different stack configurations simulated with the WVASE software at an angle of 0°. The configurations in the legend have the order of the first layer-pair, meaning that in the uneven cases the first material is added again as the last layer. Layer thicknesses are kept the same in each configuration.

For real applications, the DBRs are designed based on the zero-angle case, and even though it is possible to model this with the WVASE software, the lowest angle that can actually be measured with the ellipsometer is 15-degrees.

4 Transfer matrix method in MATLAB

In section 2.3 the theoretical basic overview of the TMM method was given. In reality the implementation of this method is a bit more complicated if the aim is using coding software to generate results. There are multiple great commercial softwares like WVASE, SETFOS and Lumerical that have the TMM implemented in them, and they utilize it to model optical properties of multilayer structures. This thesis aims to develop a MATLAB code that can be quickly used to model the reflectivity spectrum of a DBR. For this purpose, the handling of electrical fields was left out and the only focus is on the reflectivity. Some existing TMM codes are available for MATLAB,[32,33] and they implement many more calculated properties and possible component architectures than the code developed for this thesis, but lack in clarity and good coding principles.

4.1 Procedure to implement DBR modeling in MATLAB

The overall procedure to implement the code is somewhat simple, and here an overview of the main script is given:

1) Load refractive index data for both materials and the substrate used as a function of wavelength.
2) Create variables for:
    a. thickness of high index layers
    b. thickness of low index layers
    c. refractive index of the surrounding medium i.e. air
    d. number of layer pairs N
    e. polarization type, either ‘s’ or ‘p’
3) Create arrays for:
    a. desired wavelength range
    b. desired angles of incidence values
4) Interpolate refractive index data to match the chosen wavelength range.
5) Loop over the angle values and inside the loop:
    a. Call the transfer matrix function
    b. Plot reflectivity values against wavelength values

The main functional difference here compared to the other codes is the addition of a wavelength range and with it the ability to take into account the dispersion of the refractive index. The transfer matrix method is implemented as a separate function, like in the other codes, but here it is called inside a for-loop to enable modeling multiple angles in a single simulation. This method obviously does require the refractive indices of the materials as a function of wavelength in a tabulated form.

4.2 TMM function

The idea behind constructing a simpler and cleaner version of the existing MATLAB codes was to focus purely on the system matrix with Fresnel coefficients to account the partial reflections from interfaces and wave vectors to account for phase changes during the light beam path in the mediums. These are enough for modeling the partial reflections happening inside the stack. This process is affected by the thicknesses and refractive indices of the layers. Since the structure is periodical, the refraction angles can be easily calculated using Snell's law[13,20–22]:

$$\theta_1 = \sin^{-1}\left(\frac{n_0 \cdot \sin\theta_0}{n_1}\right)$$

$$\theta_2 = \sin^{-1}\left(\frac{n_0 \cdot \sin\theta_0}{n_2}\right)$$

Here the subscripts represent the layers, 0 refers to air before the stack, 1 refers to layer one and 2 refers to layer two. In both cases we can use the incident angle and refractive index of air as a reference since the angle to the normal of the stack after an SiO_2 interface is the same whether light has come from air or Ta_2O_5:

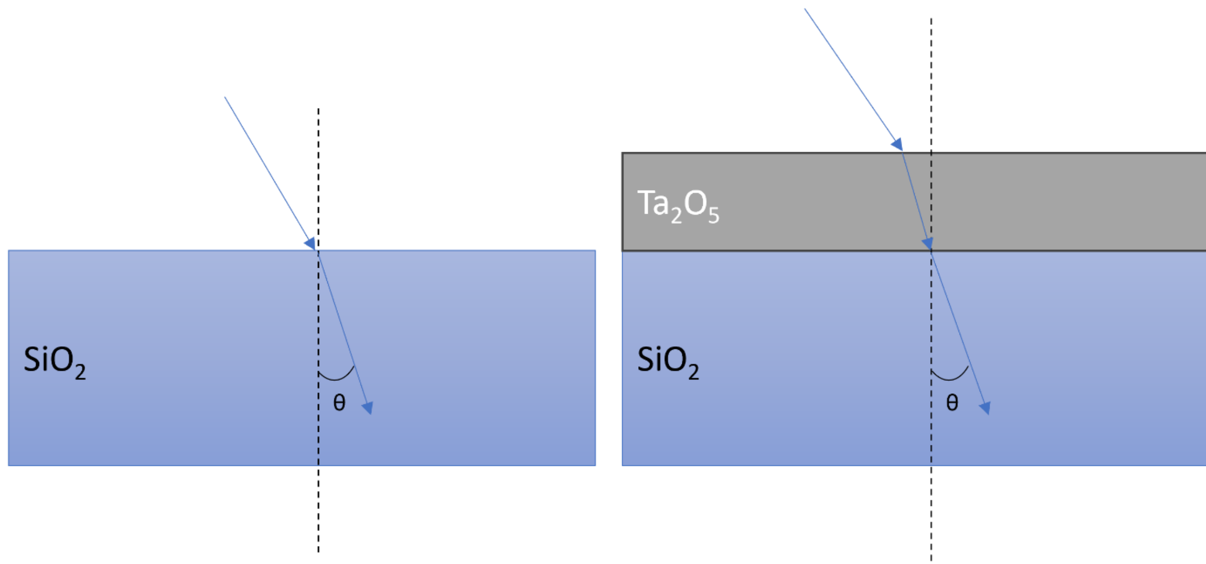

Figure 19: Refraction angle θ of the light compared to the normal of the stack would be the same in both cases in the SiO_2 layer.

The phase changes can be accounted for by using the wave vectors of the layers[13,20–22]:

$$k_0 = \frac{2\pi}{\lambda}$$

$$k_{1z} = k_0 \cdot n_1 \cdot \cos\theta_1$$

$$k_{2z} = k_0 \cdot n_2 \cdot \cos\theta_2$$

Then the matrices for the two material layers for s-polarization are:

$$M_{1,s} = \begin{pmatrix} \cos(k_{1z} \cdot d_1) & \dfrac{i \cdot \sin(k_{1z} \cdot d_1)}{n_1 \cdot \cos(\theta_1)} \\ i \cdot n_1 \cdot \cos(\theta_1) \cdot \sin(k_{1z} \cdot d_1) & \cos(k_{1z} \cdot d_1) \end{pmatrix}$$

$$M_{2,s} = \begin{pmatrix} \cos(k_{2z} \cdot d_2) & \dfrac{i \cdot \sin(k_{2z} \cdot d_2)}{n_2 \cdot \cos(\theta_2)} \\ i \cdot n_2 \cdot \cos(\theta_2) \cdot \sin(k_{2z} \cdot d_2) & \cos(k_{2z} \cdot d_2) \end{pmatrix}$$

And for p-polarization:

$$M_{1,p} = \begin{pmatrix} \cos(k_{1z} \cdot d_1) & \dfrac{i \cdot \sin(k_{1z} \cdot d_1) \cdot \cos(\theta_1)}{n_1} \\ i \cdot \dfrac{n_1}{\cos(\theta_1)} \cdot \sin(k_{1z} \cdot d_1) & \cos(k_{1z} \cdot d_1) \end{pmatrix}$$

$$M_{2,p} = \begin{pmatrix} \cos(k_{2z} \cdot d_2) & \dfrac{i \cdot \sin(k_{2z} \cdot d_2) \cdot \cos(\theta_2)}{n_2} \\ i \cdot \dfrac{n_2}{\cos(\theta_2)} \cdot \sin(k_{2z} \cdot d_2) & \cos(k_{2z} \cdot d_2) \end{pmatrix}$$

The refractive index and angle of incidence have effects on the phase change while the light is propagating in the materials which is accounted for in the wave vectors, they also have effects on the interfaces, which is why they are used as terms again in the matrices. After obtaining the layer matrices, it is a simple multiplication of all the matrices together, depending on how many layers there are in the DBR structure:

$$M_{period,s} = M_{1,s} \cdot M_{2,s} \rightarrow M_{total,s} = {M_{period,s}}^N$$

Where N is the number of layer pairs. In a case of odd number of layers, the total matrix would be multiplied once more with the matrix of the first layer, $M_{1,s}$. To account the first interface between air and layer 1, as well as the last interface between the last layer and the substrate, we construct corresponding matrices for those interfaces[2,13]:

$$I_0 = \begin{pmatrix} 1 & 1 \\ \dfrac{n_0}{\cos(\theta_0)} & \dfrac{n_0}{-\cos(\theta_0)} \end{pmatrix}$$

$$I_s = \begin{pmatrix} 1 & 1 \\ \dfrac{n_s}{\cos(\theta_s)} & \dfrac{n_s}{-\cos(\theta_s)} \end{pmatrix}$$

After this the total system matrix is:

$$S = I_0 \cdot M_{total,s} \cdot I_s$$

And from this the reflectivity value is[2,13,21,22]:

$$R = \left| \frac{S(2,1)}{S(1,1)} \right|^2$$

5 Results & Discussion

This chapter discusses the effects of deposition parameters based on literature findings and experimental results. The results of the deposition parameter optimization and the performance of the developed MATLAB code are presented and analysed.

5.1 Optimization of deposition time

Optimizing deposition parameters is done to achieve an acceptable balance between deposition time and film quality. Achieving uniform films of good quality is pivotal for optical components, which is expected when using physical vapor deposition methods. The key parameters influencing thin film deposition in sputtering are the power used, process pressure and gas flows into and out of the chamber during the deposition process. This chapter discusses their effects based on literature findings and experimental results.

As shown in Table 1 in the section 4.1, the deposition rates for the initially used recipes were 0.33 Å/s for SiO_2 and 0.51 Å/s for Ta_2O_5. Fabrication of a 6-pair DBR targeted at 550 nm stopband center with these rates would consist of a total time for the depositions of 405 minutes which is almost 7 hours. On top of this it always takes some time for the machine to switch between the recipes. Process pressure was found to be the most important parameter to optimize and a 1 mTorr value was found to be the best for deposition rate on both materials. Sputtering power should be kept as high as possible, but it can lead to damage in the targets.

5.1.1 Sputtering power

The sputtering power is expressed as a percentage of the maximum power available in the system which for this particular evaporator is 600 W. The maximum power that can be used for a particular material is provided by the manufacturers of the targets and are expressed as power per surface area. Since increasing the sputtering power corresponds linearly with the sputtering yield and larger powers result in more uniform and compact film structures, it makes sense to keep the used power at the maximum.[27,28] However there are two caveats to this:

1) Sputtering power impacts the refractive index *n.*
2) More power results in harsher conditions at the target during deposition and can lead to faster wearing in the targets.

Point 1) gives rise to a possibility of using lower power during the deposition of SiO_2 because it is the lower index material, thus leading to a larger contrast between the refractive indices of the films. Zhao et al.[28] did a study on the effects of radio frequency sputtering power on SiO_2 films and found that the refractive index actually decreases when lowering the sputtering power. They performed stoichiometric studies on the films and found that the molar ratio of O/Si increased from 1.87:1 to 1.99:1 when the power decreased from 150 W to 60 W. The latter is practically the ideal ratio of SiO_2. This could be used as a way to achieve lower index films.

Point 2) obviously is a frustrating consequence to observe, since the sputtering targets are expensive and it is not ideal to ideal to push them above their limits. Since the maximum power limits are provided by the manufactures and theory, the targets should be able to handle these deposition conditions for an adequate amount of time. The maximum output power used for a target can be calculated by multiplying the manufacturer provided *maximum power density per target* with the surface area of the target disc. For example, the used three-inch diameter SiO_2 target has a maximum power density of 30 watts per square inch:

$$\pi \cdot (1.5\ in)^2 \cdot 30 \frac{W}{in^2} = 212\ W$$

This is about 35% of the 600 W that the evaporators power source can provide. During this project, the SiO_2 target was changed once and some indium bonding leakage was observed; however, this did not yet affect the sputtering process harmfully in terms of resulting film quality. This caused abortions in the sputtering processes, causing unwanted delays. A probable cause for this is that during the project, the deposition rate for the Ta_2O_5 films was increased by a factor of 175%, and this led to the SiO_2 target not having enough time to cool down during subsequent depositions in the DBR stack fabrication.

The range in deposition rate during separate deposition was observed to be quite minimal, however if the sputtering system has not been well maintained and cleaned, there can be problems with the physical sensors. This could lead to a large deviation in actual thickness especially in the case of SiO_2 since its deposition takes a longer time.

5.1.2 Process pressure

As the goal of the project was to decrease the fabrication time of DBRs, and for this purpose, it was reasonable to keep the sputtering power as high as possible, the logical parameter to investigate was the pressure during deposition. As per sputtering theory, lower pressure means

fewer collisions in the plasma cloud and higher energies of particles coming off from the target, which should lead to faster deposition of films. Accordingly, this was observed up until 1 mTorr pressures, leading to faster deposition times especially for Ta_2O_5. The deposition rate increased from 0.5 to 1.4 Å/s. In the case of SiO_2, the improvement was insignificant. Going below 1 mTorr, the deposition rates started to decrease and for SiO_2 a significant deviation from the target thickness was observed.

Table 3: Sputtering parameters and corresponding deposition rates and measured thicknesses.

	Power [%]	Pressure [mTorr]	Ar Flow [SCCM]	O_2 Flow [SCCM]	Rate [Å/s]	Target thickness [nm]	Measured Thickness [nm]
SiO_2	30	5	15	0	0.33	60	61.3 ± 0.2
SiO_2	30	1	15	0	0.39	60	55.4 ± 0.1
SiO_2	30	0.5	15	0	0.27	60	46.4 ± 0.2
Ta_2O_5	45	5	20	10	0.51	60	57.6 ± 0.1
Ta_2O_5	45	1	20	10	1.4	60	59.3 ± 0.1
Ta_2O_5	45	0.5	20	10	1.12	60	59.6 ± 0.1

At higher pressures the plasma is denser and this leads to more collisions for the ejected target atoms on their way to the substrate. These collisions are unwanted and decrease the number of particles reaching the substrate as well as decrease the kinetic energy they have resulting in lower rates. Going below 1 mTorr pressure the deposition rates started decreasing, meaning that the ideal conditions are around 1 mTorr. Lower process pressure means that the argon plasma is less dense leading to a smaller sputtering yield and thus smaller deposition rate. Another impacting factor with lower pressures comes from the deposition system itself. To maintain the process pressure, there needs to be an outflow of the gases involved, and with lower pressures this outflow is faster. Interestingly, with SiO_2, the measured thickness was significantly lower than the target thickness, and this deviation shows an increasing trend when lowering the process pressure. For Ta_2O_5 the measured thicknesses were consistent throughout different deposition conditions. Silicon has much smaller mass compared to tantalum and this can cause the effects of the surrounding environment to have larger impacts on the silicon atoms. The high deviation of the measured thickness from the target thickness in the 0.5 mTorr deposition could be explained by already deposited atoms being knocked off from the substrate due to

higher kinetic energies of the particles involved. For tantalum, which has a larger mass, these effects would be smaller, which explains the consistency. One possible reason could also be the additional O_2 flow that allowed oxygen atoms to deposit. This would have led to a deviation from the ideal stoichiometric ratio, however there was no change in measured refractive index values which are plotted in Figure 20.

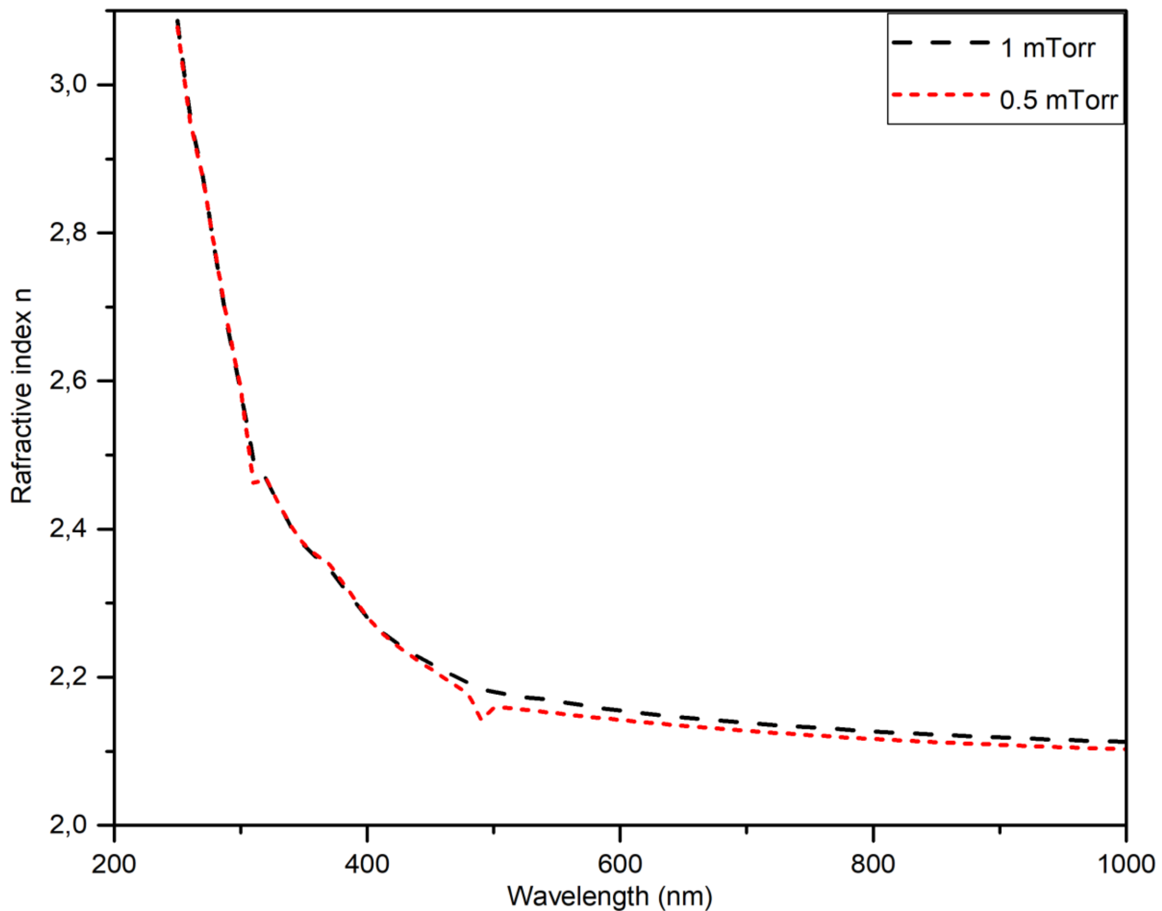

Figure 20: Measured n-values for 1 and 0.5 mTorr depositions of Ta2O5.

Taking into account the increasing deviations from target thickness and a relatively low increase in deposition rate for SiO_2 while having observed the damaging of the sputtering target, it could be a useful practice to accept the longer deposition times.

5.1.3 Gas flows

Gas flow parameters of the initial recipes used were found to be already optimized in this sputtering set up. In the case of Ta_2O_5, adjusting the O_2 to argon ratio led to large deviations from target thickness and a significant increase in absorption in the visible range. Reducing the O_2 to argon ratio led to a high deposition rate of 2.01, but this caused lower transmissivity of

the resulted films. This could be due to either absorption or scattering effects from defects in the material. With SiO_2, a change in argon flow or introducing additional O_2 flow led to the deposition rate dropping below 0.2 Å/s. Using a SiO_2 target instead of pure Si target negates the need for a reactive gas. According to Franke et al.[34,35], with lower oxygen ratios tantalum forms Ta-Ta metallic clusters in what is called metallic sputtering regime and this causes absorption in the visible range. When going to higher oxygen ratios the resulting film closes in to the ideal stoichiometric ratio but can start to cause "poisoning of the target surface"[24] leading to a sudden drop in deposition rate. For a more in depth discussion on the gas flow effects and different sputtering regimes refer to "Fundamental understanding and modeling of reactive sputtering processes"[24] and "Control of reactive sputtering processes"[36].

5.2 Refractive indices

The main optical property of a material involving DBR utilization is the refractive index *n* and its imaginary component the extinction coefficient *k*. As the names suggest, the goal is to find a large index material to be used as the high index layers, and the opposite goes to the lower index material. It is also important to use materials with low absorption, zero if possible, to maximize the reflectivity. It would hinder the function of a DBR if the light was absorbed inside the stack where the partial reflections travel back to the surface. Figures 21 and 22 represent the *n* and *k* values for SiO_2 and Ta_2O_5, respectively, with data from two different sources and from the in-house fabricated thin films. The measured values are from 1 mTorr depositions and the general oscillator layers were constructed from those measured values with the WVASE software. As can be seen, the generated data is in excellent agreement with the reference data in both cases. When it comes to the extinction coefficient of SiO_2, the scale is low enough to justify accounting the differences to noise. For both materials all the data suggests a near zero absorption throughout the visible wavelength range, which is one major reason for choosing these materials.

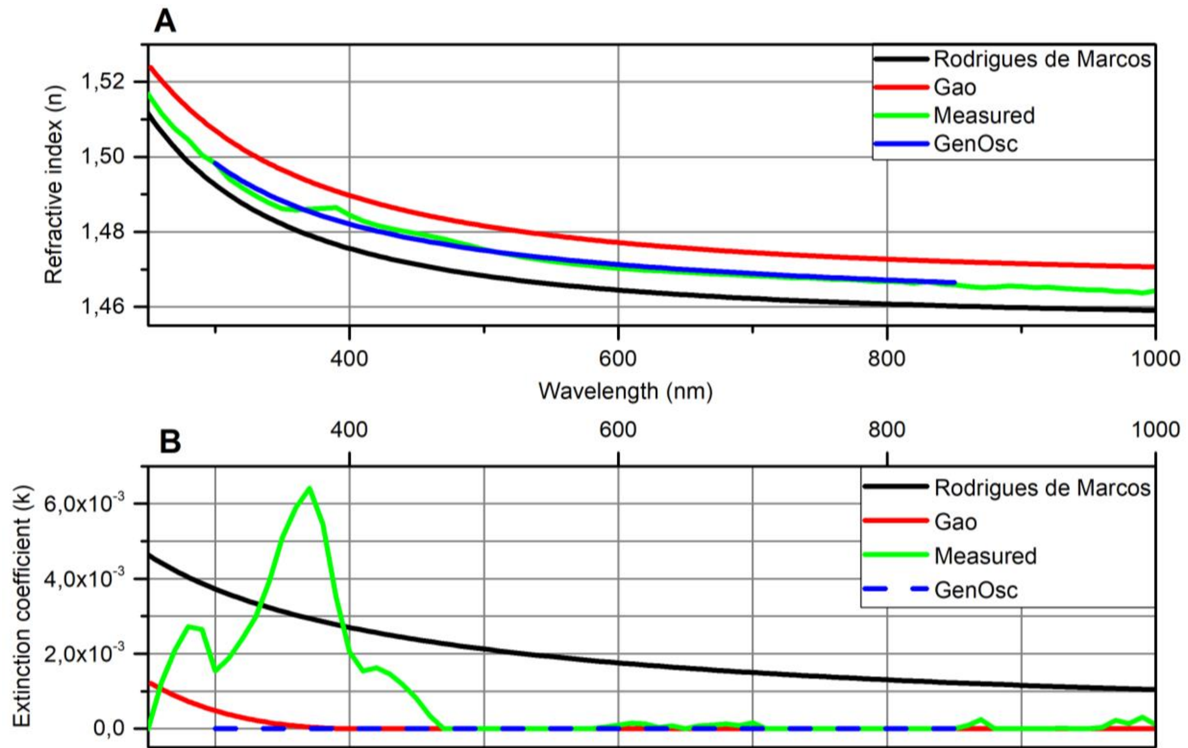

Figure 21: Optical constants (A: refractive index n, B: extinction coefficient k) for SiO_2 from measured films and the general oscillator layers built from the measured values compared with two reference sources[29,30].

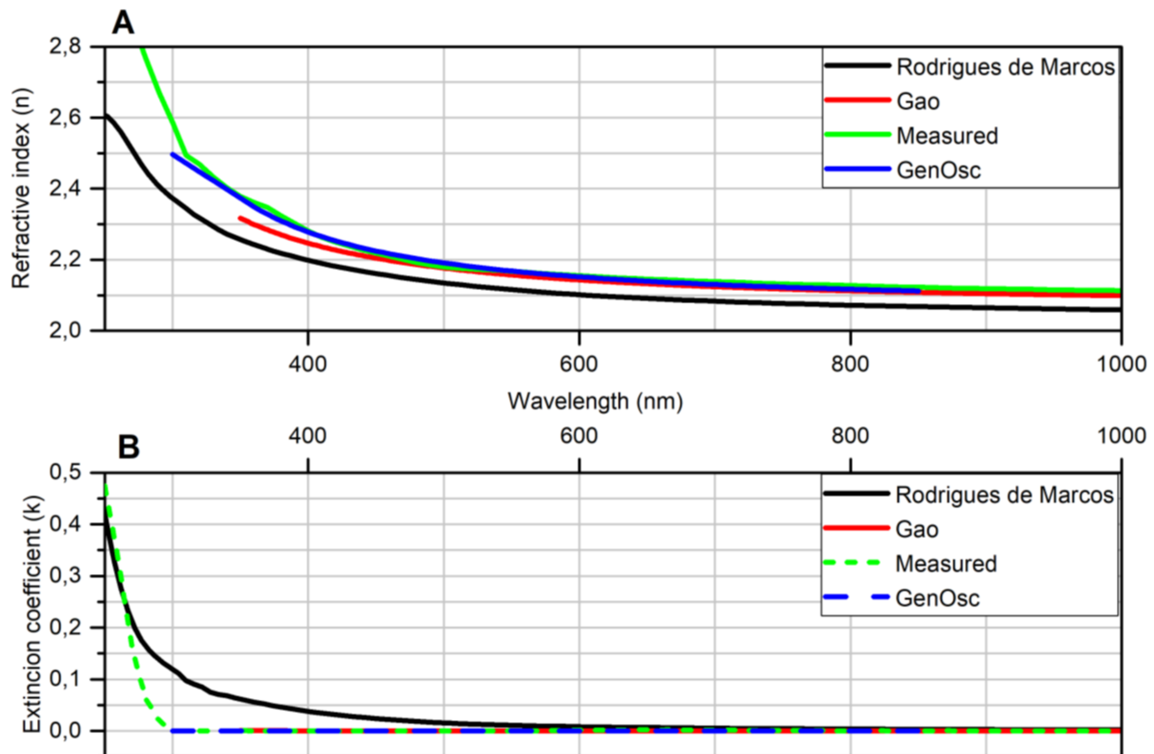

Figure 22: Optical constants (A: refractive index n, B: extinction coefficient k) for Ta_2O_5 from measured films and the general oscillator layers built from the measured values compared with two reference sources[29,37].

As mentioned earlier in the theory part, the refractive index contrast between the two materials in a DBR stack is pivotal in getting larger reflectivity values with fewer number of pairs. This is especially essential when manufacturing devices with physical vapor deposition methods since the process is time-consuming. Figure 23 shows the refractive index contrast of the two materials from the generated general oscillator layers. The difference grows larger towards shorter wavelengths, which leads to higher reflectivity and thus a slight skewing of the reflection spectrums to the lower wavelengths.

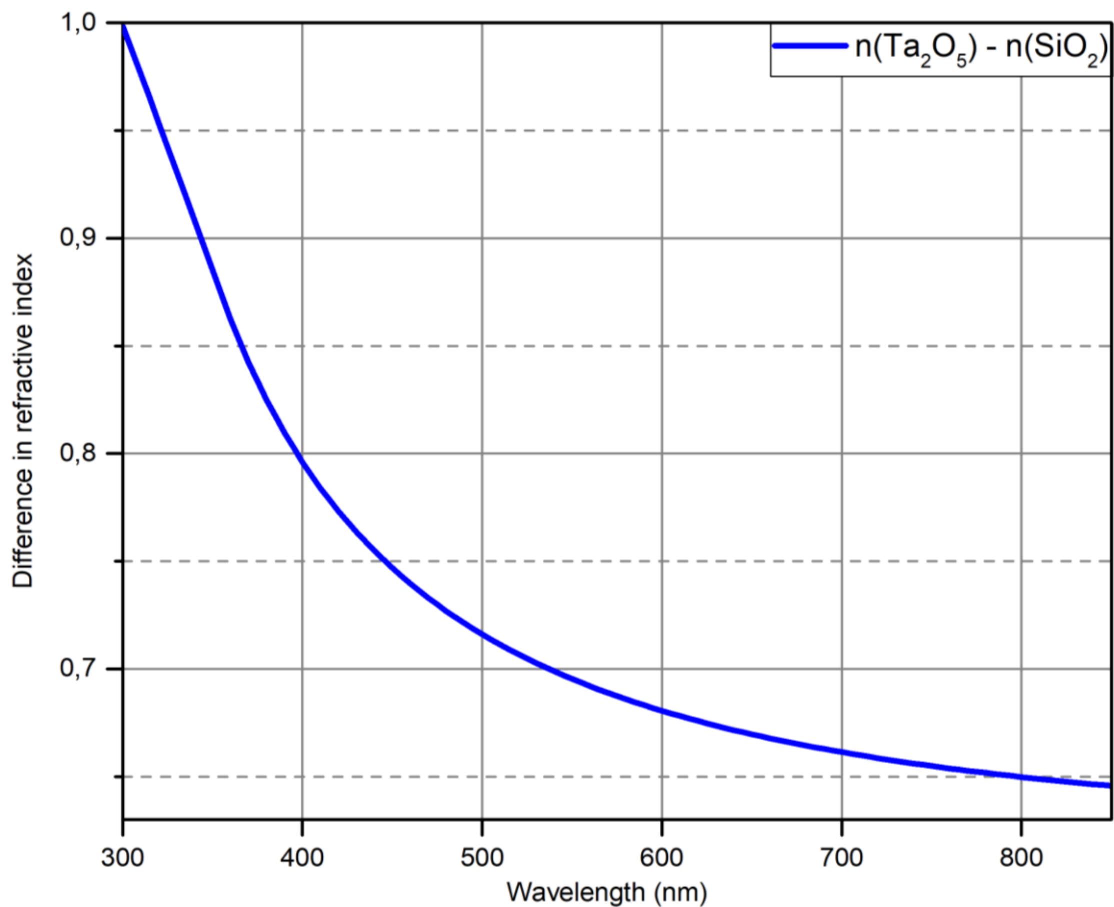

Figure 23: Refractive index contrast of SiO_2 and Ta_2O_5 calculated from the general oscillator models built with the WVASE software from measured values.

5.3 Reflectivity of deposited distributed Bragg reflectors

The maximum theoretical reflectivity using n-values at 550 nm of 6-pair DBRs at 0-degree angle of incidence as is given by equation (17) is 0.962. In Table 4 below are the maximum reflectivities and corresponding wavelength values of two different DBR structures with three different generation methods: simulating with WVASE and MATLAB as well as actual measurements from fabricated samples. As mentioned in the theory chapter of DBRs the

maximum reflectivity equation (17) does not hold for the uneven number of layer-pair stacks. If the equation is used for a 5.5 pair DBR, the result is 0.945, which is lower than both the generated and measured values for that stack configuration.

Table 4: Maximum reflectivities for two different stack configurations and corresponding wavelengths. In all configurations the layer thicknesses of the corresponding materials are kept the same.

6 pairs SiO_2 - Ta_2O_5	R_{max}	λ at R_{max} (nm)
Generated WVASE at 0°	0.974	547
Generated MATLAB at 0°	0.962	550
Generated WVASE at 15°	0.977	542
Generated MATLAB at 15°	0.967	541
Measured at 15°	0.966	550
5.5 pairs Ta_2O_5 - SiO_2		
Generated WVASE at 0°	0.974	547
Generated MATLAB at 0°	0.982	547
Generated WVASE at 15°	0.978	542
Generated MATLAB at 15°	0.984	542
Measured at 15°	0.977	534

The constructed MATLAB code is highly accurate and all the reflectivities match the theory nicely with the exception that WVASE generated data shows a slightly higher maximum reflectivity at 0° and there are small deviations in the Bragg modes. MATLAB matching the theory exactly is expected as it is an ideal case since using only the Fresnel coefficients to calculate and model the reflectivity spectrum. All in all, the reflectivity values are very close to each other in all cases and some rounding errors at this accuracy could happen. The measured reflectivity maximums wavelength location indicates high accuracy in the deposited layer thicknesses. Figures 24, 25 and 26 illustrate the spectrums of multiple different configurations and it is found that the best reflectivities are achieved with the 5.5-layer pair Ta_2O_5 - SiO_2 - Ta_2O_5 configuration.

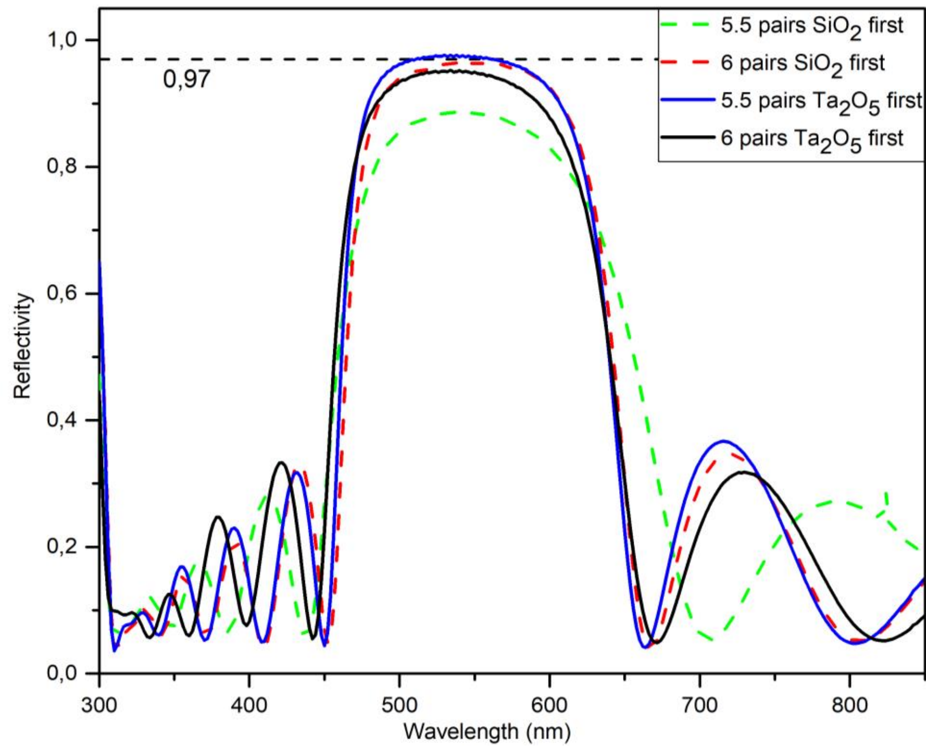

Figure 24: Measured reflectivity spectrums for four different stack configurations at 15°. Target layer thicknesses for all configurations were kept the same.

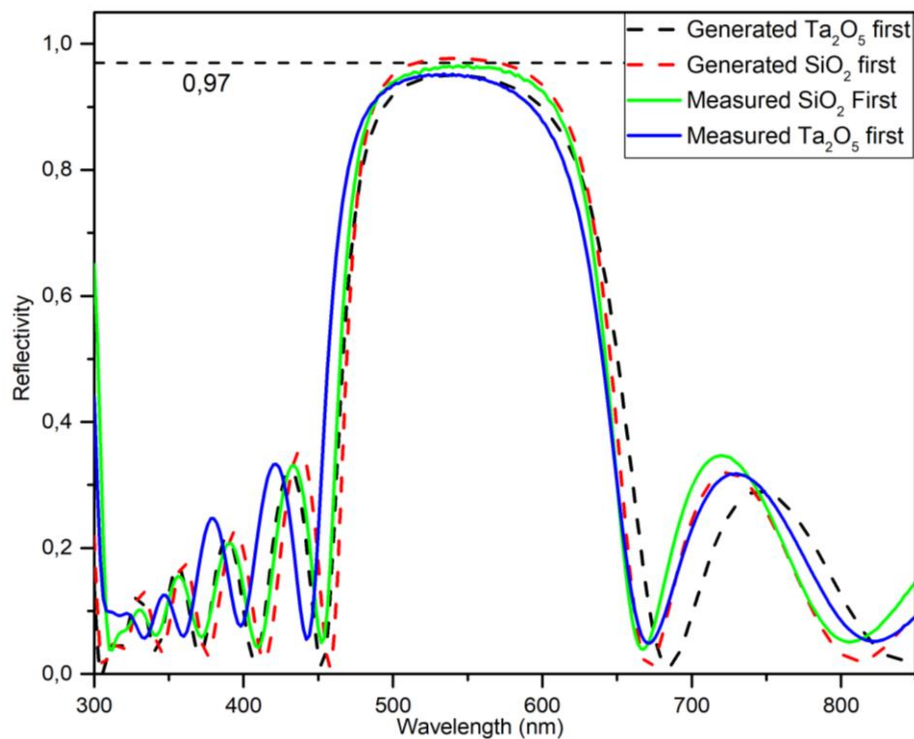

Figure 25: Comparison between measured and WVASE generated reflectivity spectrums for two different stack configurations of 6 layer-pair DBRs at 15°. In all configurations the layer thicknesses of the corresponding materials are kept the same.

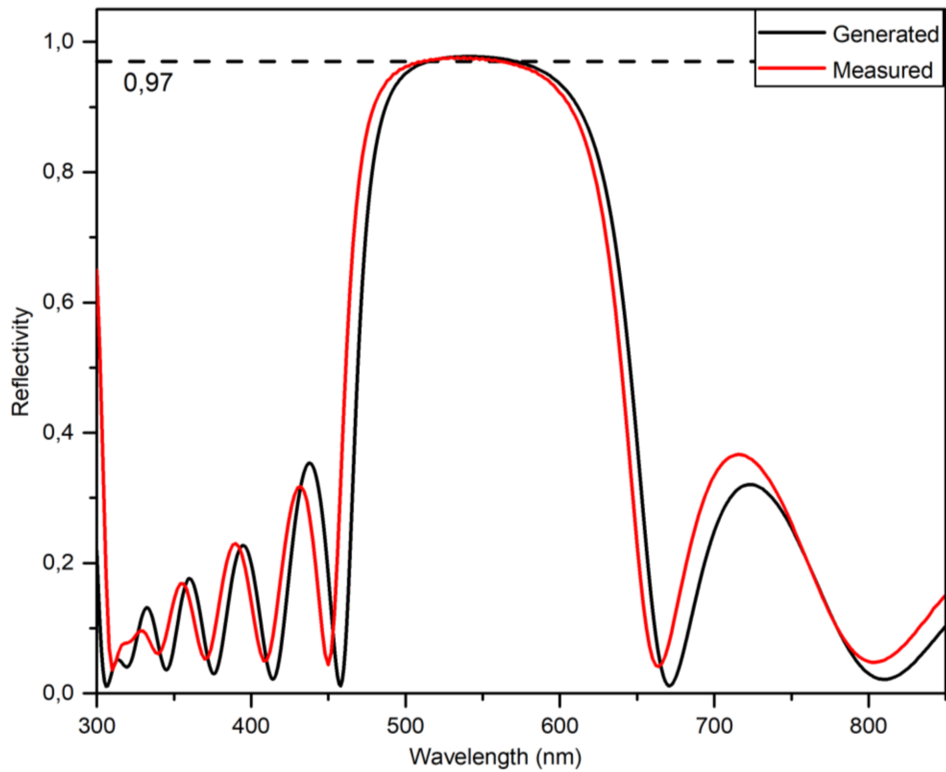

Figure 26: Measured and WVASE generated reflectivity spectrums at 15° of a 5.5 pair DBR with Ta_2O_5 as the first and last layer.

Overall, the MATLAB code developed matches WVASE simulations quite nicely, however there are some deviations in the intensities of the Bragg modes in both sides of the main stopband. In p-polarization there is increasing deviation also on the main stopband shape with increasing angle. The performance of the developed MATLAB code against WVASE simulations is illustrated in Figure 27.

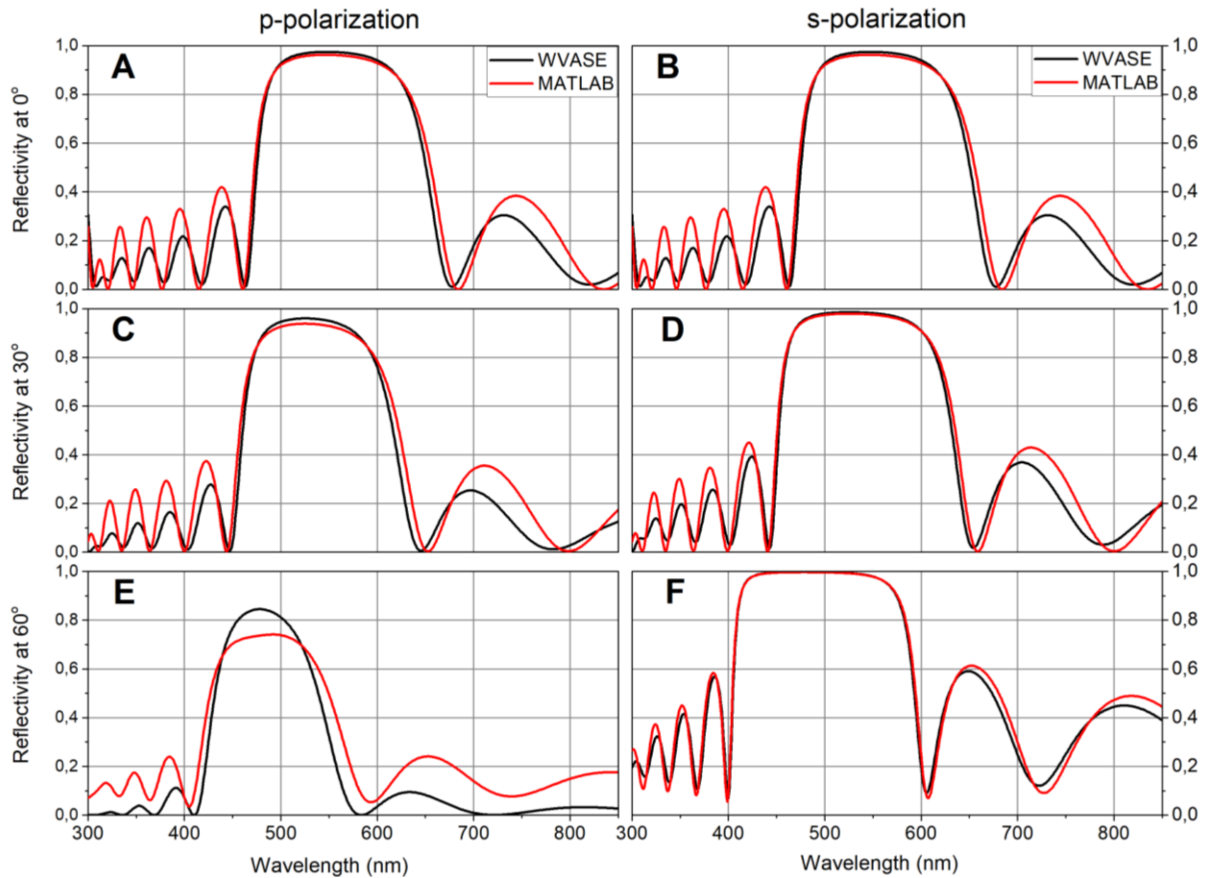

Figure 27: Generated reflectivity spectrums using WVASE and the built MATLAB code for the same 6-layer pair stack. The left column contains p-polarization and the right column s-polarization. A and B are at 0° angle of incidence, C and D are at 30°, and E and F are at 60°.

Interestingly, when comparing the MATLAB code and WVASE modeling to one of the referenced codes[33] the MATLAB code matches WVASE better in terms of the peak reflectivity of the stopband:

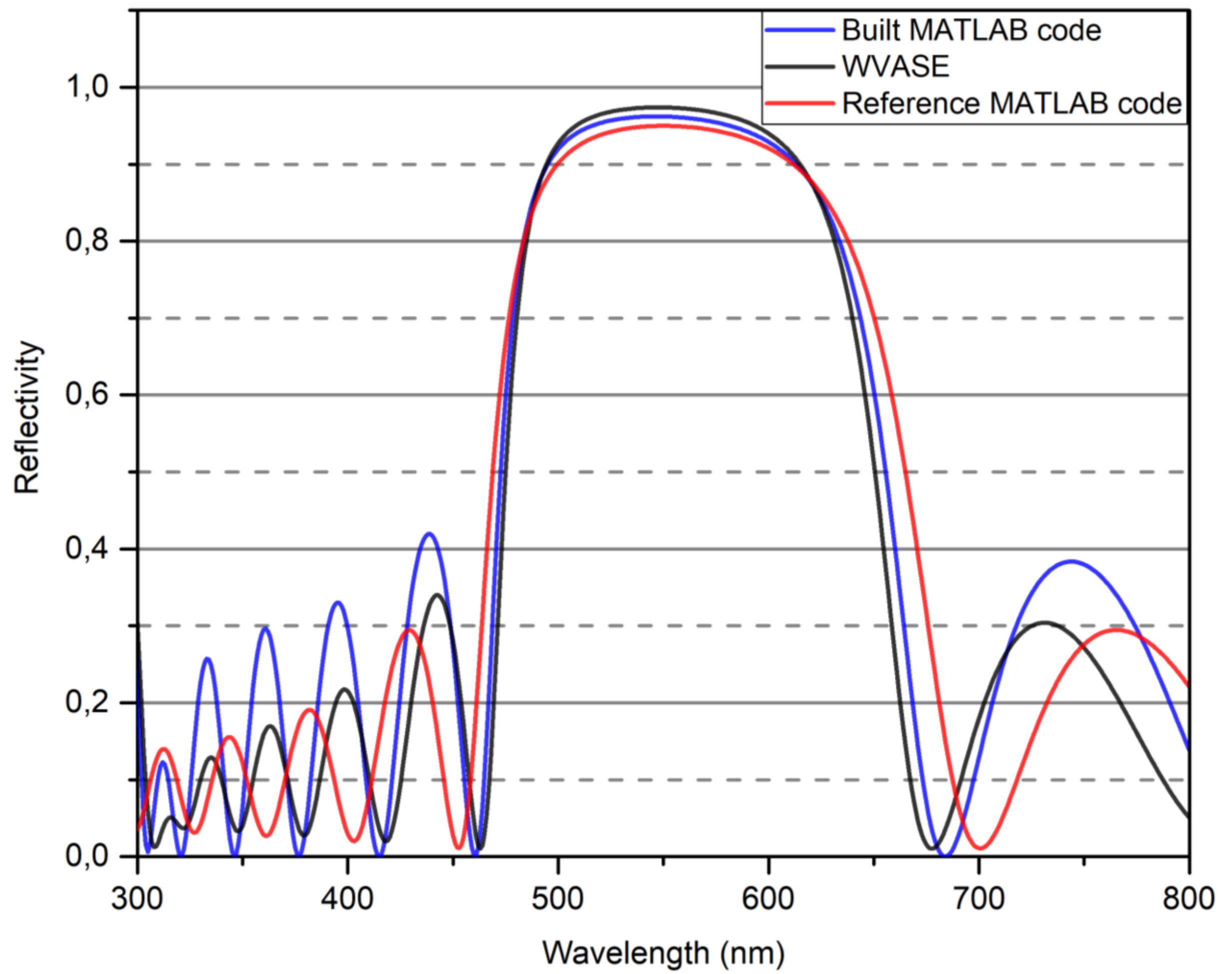

Figure 28: Comparison of three differently simulated reflectivity spectrums of six layer-pair DBRs with Ta_2O_5 as the final layer. Presented are two different MATLAB generated spectrums, one with the code developed for this thesis and the other is from 1D Light Wave Transmission[33].

6 Conclusions

In this thesis distributed Bragg reflectors of multiple different stack configurations were fabricated by sputtering using SiO_2 and Ta_2O_5. The DBRs were characterized and modelled using two different softwares: MATLAB and WVASE. The deposition parameters for both materials were optimized for EvoVac720 evaporator from Ångstrom engineering. It was found that 1 mTorr of process pressure is the optimal environment for both materials regarding the deposition rate. Sputtering power should be kept close to the maximum informed by the manufacturer of the sputtering targets, however if the SiO_2 target used has indium bonding between the target and a copper backplate, this might result in faster deterioration of the target. Deposition rate for Ta_2O_5 was increased by 175% and for SiO_2 by 20%. Fabricated films were of extremely high quality achieving high reflectivities and wide stopbands using only 5.5- and 6-layer pairs. The reflectivity spectrums of fabricated structures matched well with simulations.

A novel MATLAB code was developed to simulate the reflectivity spectrums of DBRs with the implementation of refractive index dispersion as a function of wavelength. The developed code achieves the goal of being more simplistic and easier to read and modify compared to existing open-source codes. This is achieved by using just the Fresnel coefficients to model reflectivity and omitting electrical field modeling from the simulations. The resulting reflectivity spectrums match closely with experimental data and existing modeling software when used at low angles of incidence. When simulating p-polarization at higher angles the MATLAB code starts to significantly deviate from the corresponding results by the established commercial WVASE software.

Overall, this thesis contributes to the theoretical understanding and modeling of DBRs and offers a novel simulation tool that is simple yet effective in visualizing reflectivity spectrums of DBRs. The importance of optimizing deposition parameters is demonstrated not only in achieving high-quality thin films but also in accelerating the deposition process in a PVD-method.

References

1. Lova, P., Manfredi, G. & Comoretto, D. Advances in Functional Solution Processed Planar 1D Photonic Crystals. *Adv. Opt. Mater.* **6**, 1800730 (2018).
2. Thin-Film Optical Filters by H. A. MacLeod: Moyen Hardcover (1986) | Ammareal. https://www.abebooks.co.uk/9780852747841/Thin-Film-Optical-Filters-Series-Optics-0852747845/plp.
3. Klingshirn, C. F. Interaction of Light with Matter. in *Semiconductor Optics* (ed. Klingshirn, C. F.) 39–75 (Springer, Berlin, Heidelberg, 2012). doi:10.1007/978-3-642-28362-8_3.
4. Palo, E. & Daskalakis, K. S. Prospects in Broadening the Application of Planar Solution-Based Distributed Bragg Reflectors. *Adv. Mater. Interfaces* **10**, 2202206 (2023).
5. J.A. Woollam Co., Inc. Guide to Using WVASE32. (2010).
6. Hecht, E. *Optics, 4e*. (Pearson Education India).
7. Born, M. & Wolf, E. *Principles of Optics: Electromagnetic Theory of Propagation, Interference and Diffraction of Light*. (Cambridge University Press, Cambridge, 1999). doi:10.1017/CBO9781139644181.
8. William D Callister, J. & David G Rethwisch. *Materials Science and Engineering: An Introduction*. (Wiley, 2018).
9. Young, H. D. *Sears and Zemansky's University Physics with Modern Physics*. (Pearson, Harlow, United Kingdom, 2020).
10. Saleh, B. E. A. & Teich, M. C. *Fundamentals of Photonics*. (2007).
11. Banning, M. Practical Methods of Making and Using Multilayer Filters. *JOSA* **37**, 792–797 (1947).

12. Daskalakis, K. S., Freire-Fernández, F., Moilanen, A. J., van Dijken, S. & Törmä, P. Converting an Organic Light-Emitting Diode from Blue to White with Bragg Modes. *ACS Photonics* **6**, 2655–2662 (2019).

13. Orfanidis, S. J. Electromagnetic Waves and Antennas. *Electromagn. Waves* (2004).

14. Wilmsen, C. W., Temkin, H. & Coldren, L. A. *Vertical-Cavity Surface-Emitting Lasers: Design, Fabrication, Characterization, and Applications*. (Cambridge University Press, 2001).

15. Abe, I. Y., Mazzeo, A., Ferlauto, A. S., Alayo, M. I. & Melo, E. G. Inverse design of distributed bragg reflector targeting a sharp reflectivity spectrum. *Photonics Nanostructures - Fundam. Appl.* **57**, 101183 (2023).

16. Tatum, J. A. *et al.* VCSEL-Based Interconnects for Current and Future Data Centers. *J. Light. Technol.* **33**, 727–732 (2015).

17. Yu, H. *et al.* Progress and prospects of GaN-based VCSEL from near UV to green emission. *Prog. Quantum Electron.* **57**, 1–19 (2018).

18. Haldar, A., Reddy, M. S. & Vijaya, R. Enhancement of light collection through flexible polymeric films patterned using self-assembled photonic crystals. *J. Phys. Appl. Phys.* **48**, 265103 (2015).

19. Betancur, R. *et al.* Transparent polymer solar cells employing a layered light-trapping architecture. *Nat. Photonics* **7**, 995–1000 (2013).

20. Berkhout, A. & Koenderink, A. F. A simple transfer-matrix model for metasurface multilayer systems. *Nanophotonics* **9**, 3985–4007 (2020).

21. Katsidis, C. C. & Siapkas, D. I. General transfer-matrix method for optical multilayer systems with coherent, partially coherent, and incoherent interference. *Appl. Opt.* **41**, 3978–3987 (2002).

22. Troparevsky, M. C., Sabau, A. S., Lupini, A. R. & Zhang, Z. Transfer-matrix formalism for the calculation of optical response in multilayer systems: from coherent to incoherent interference. *Opt. Express* **18**, 24715–24721 (2010).

23. Developing Solution-Processed Distributed Bragg Reflectors for Microcavity Polariton Applications | The Journal of Physical Chemistry C. https://pubs.acs.org/doi/full/10.1021/acs.jpcc.3c01457.

24. Berg, S. & Nyberg, T. Fundamental understanding and modeling of reactive sputtering processes. *Thin Solid Films* **476**, 215–230 (2005).

25. Gudmundsson, J. T. & Lundin, D. 1 - Introduction to magnetron sputtering. in *High Power Impulse Magnetron Sputtering* (eds. Lundin, D., Minea, T. & Gudmundsson, J. T.) 1–48 (Elsevier, 2020). doi:10.1016/B978-0-12-812454-3.00006-1.

26. Magnetron Sputtering Overview. *Angstrom Engineering* https://angstromengineering.com/tech/magnetron-sputtering/.

27. Chen, X., Bai, R. & Huang, M. Optical properties of amorphous Ta2O5 thin films deposited by RF magnetron sputtering. *Opt. Mater.* **97**, 109404 (2019).

28. Zhao, C., Zhao, L., Liu, J., Liu, Z. & Chen, Y. Effect of sputtering power on the properties of SiO2 films grown by radio frequency magnetron sputtering at room temperature. *Opt. Quantum Electron.* **53**, 15 (2021).

29. Marcos, L. V. R., Larruquert, J. I., Méndez, J. A. & Aznárez, J. A. Self-consistent optical constants of SiO_2 and Ta_2O_5 films. *Opt. Mater. Express* **6**, 3622–3637 (2016).

30. Gao, L., Lemarchand, F. & Leguime, M. Refractive index determination of SiO2 layer in the UV/Vis/NIR range: spectrophotometric reverse engineering on single and bi-layer designs. *J. Eur. Opt. Soc.* **8**, 8 (2013).

31. Klingshirn, C. F. Kramers–Kronig Relations. in *Semiconductor Optics* (ed. Klingshirn, C. F.) 129–134 (Springer, Berlin, Heidelberg, 2012). doi:10.1007/978-3-642-28362-8_6.

32. Shawn Divitt (2025). jreftran - A layered thin film transmission and reflection coefficient calculator (https://www.mathworks.com/matlabcentral/fileexchange/50923-jreftran-a-layered-thin-film-transmission-and-reflection-coefficient-calculator), MATLAB Central File Exchange. Retrieved February 5, 2025.

33. Laurent NEVOU (2025). Light_WaveTransmission1D (https://github.com/LaurentNevou/Light_WaveTransmission1D), GitHub. Retrieved February 5, 2025.

34. Franke, E. *et al.* Dielectric function of amorphous tantalum oxide from the far infrared to the deep ultraviolet spectral region measured by spectroscopic ellipsometry. *J. Appl. Phys.* **88**, 5166–5174 (2000).

35. Franke, E., Schubert, M., Trimble, C. L., DeVries, M. J. & Woollam, J. A. Optical properties of amorphous and polycrystalline tantalum oxide thin films measured by spectroscopic ellipsometry from 0.03 to 8.5 eV. *Thin Solid Films* **388**, 283–289 (2001).

36. Sproul, W. D., Christie, D. J. & Carter, D. C. Control of reactive sputtering processes. *Thin Solid Films* **491**, 1–17 (2005).

37. Gao, L., Lemarchand, F. & Lequime, M. Exploitation of multiple incidences spectrometric measurements for thin film reverse engineering. *Opt. Express* **20**, 15734–15751 (2012).

Appendices

Appendix 1 DBR Code

```
clc,clearvars;

% Define the input parameters
n1_file = 'Processed_Ta2O5_GenOsc_nvalues.txt';  % file containing refractive
indices for high index material as a function of wavelength
n2_file = 'Processed_SiO2_GenOsc_nvalues.txt';  % file containing refractive
indices for low index material as a function of wavelength
%n1_file = 'Processed_SiO2_GenOsc_nvalues.txt';  % file containing refractive
indices for high index material as a function of wavelength
%n2_file = 'Processed_Ta2O5_GenOsc_nvalues.txt';  % file containing refractive
indices for low index material as a function of wavelength
ns_file = 'fused_silica_n&k.txt';  % file containing refractive indices for
substrate as a function of wavelength
d1 = 63.4e-9;     % thickness of material 1 (in meters)
d2 = 93.35e-9;     % thickness of material 2 (in meters)
%d1 = 93.35e-9;     % thickness of material 1 (in meters)
%d2 = 63.4e-9;      % thickness of material 2 (in meters)
n0 = 1.0;        % refractive index of the incident medium (air)
wavelengths = linspace(300e-9, 850e-9, 551);  % array of wavelengths (in meters)
angles_deg = [15];  % array of angles of incidence in degrees
polarization = 's';  % polarization type: 's' for s-polarization, 'p' for p-
polarization

% Insert the Number of full layer pairs here, in case there is a odd number
% of layer pairs ie the stack ends in the same material as it starts with,
% then the last layer is inserted in the transfer matrix function
N = 6;

% Convert angle of incidence from degrees to radians
angles_rad = deg2rad(angles_deg);

% Read refractive index data from files
data_n1 = readmatrix(n1_file);
data_n2 = readmatrix(n2_file);
data_ns = readmatrix(ns_file);
data_ns(:, 1) = data_ns(:, 1) * 1e-9;  % Convert nanometers to meters
% Interpolate refractive indices for the given wavelengths
n1 = interp1(data_n1(:, 1), data_n1(:, 2), wavelengths, 'linear', 'extrap');
n2 = interp1(data_n2(:, 1), data_n2(:, 2), wavelengths, 'linear', 'extrap');
ns = interp1(data_ns(:, 1), data_ns(:, 2), wavelengths, 'linear', 'extrap');

% Initialize figure
figure;
hold on;  % To plot multiple lines on the same figure

% Loop over each angle
for i = 1:length(angles_rad)
    theta0 = angles_rad(i);

    % Call the function to compute reflectance and transmittance
    [R, ~] = transfer_matrix_method_f(n1, n2, d1, d2, n0, ns, wavelengths, theta0,
polarization, N);

    % Plot reflectance data
    plot(wavelengths * 1e9, R, 'DisplayName', sprintf('Angle = %d°',
angles_deg(i)));
end


% Export reflectance data to a text file
```

```
%export_filename = 'Matlab_6_pairs_Ta_first_15deg.txt';
%export_data = [wavelengths' * 1e9, R'];
%writematrix(export_data, export_filename, 'Delimiter', '\t', 'WriteMode',
'overwrite');


% Customize plot
xlabel('Wavelength (nm)');
ylabel('Reflectance R');
title('Reflectance Spectrum for Different Angles');
legend('show');
grid on;
hold off;
```

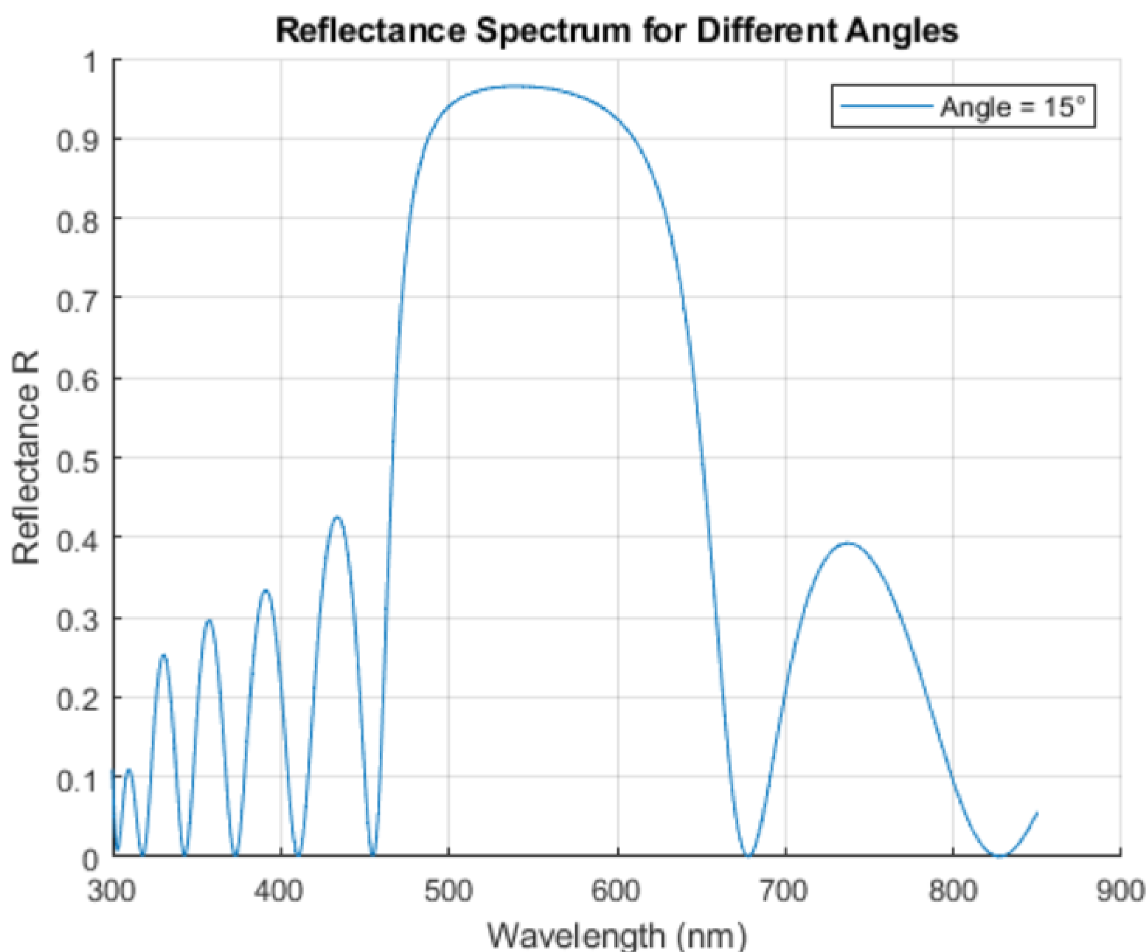

Appendix 2 Transfer Matrix Method Function

```
function [R, T] = transfer_matrix_method_f(n1, n2, d1, d2, n0, ns, wavelengths,
theta0, polarization, N)
    % Number of wavelengths to process
    num_wavelengths = length(wavelengths);

    % Preallocate arrays for reflection and transmission coefficients
    R = zeros(1, num_wavelengths);
    T = zeros(1, num_wavelengths);
```

```
    % Loop over each wavelength
    for idx = 1:num_wavelengths
        lambda = wavelengths(idx);

        % Get refractive indices for the current wavelength
        n1_idx = n1(idx);
        n2_idx = n2(idx);
        ns_idx = ns(idx);

        % Calculate the angle of refraction in each medium using Snell's law
        theta1 = asin(n0 * sin(theta0) / n1_idx);
        theta2 = asin(n0 * sin(theta0) / n2_idx);
        theta_s = asin(n0 * sin(theta0) / ns_idx);

        % Calculate wave numbers and z-components
        k0 = 2 * pi / lambda;
        k1z = n1_idx * k0 * cos(theta1);
        k2z = n2_idx * k0 * cos(theta2);
        %ksz = ns_idx * k0 * cos(theta_s);

        % Select the correct matrix based on polarization
        if strcmpi(polarization, 's')
            % s-polarization (TE mode)
            M1 = [cos(k1z * d1), 1i * sin(k1z * d1) / (n1_idx * cos(theta1));
                  1i * n1_idx * cos(theta1) * sin(k1z * d1), cos(k1z * d1)];

            M2 = [cos(k2z * d2), 1i * sin(k2z * d2) / (n2_idx * cos(theta2));
                  1i * n2_idx * cos(theta2) * sin(k2z * d2), cos(k2z * d2)];



        elseif strcmpi(polarization, 'p')
            % p-polarization (TM mode)
            M1 = [cos(k1z * d1), 1i * sin(k1z * d1) / (n1_idx / cos(theta1));
                  1i * (n1_idx / cos(theta1)) * sin(k1z * d1), cos(k1z * d1)];

            M2 = [cos(k2z * d2), 1i * sin(k2z * d2) / (n2_idx / cos(theta2));
                  1i * (n2_idx / cos(theta2)) * sin(k2z * d2), cos(k2z * d2)];
        else
            error('Invalid polarization. Use "s" for s-polarization or "p" for p-
polarization.');
        end

        % Calculate the total transfer matrix for one period
        M_period = M2 * M1;

        % Repeat the period for a stack of N layers
        M_total = eye(2);  % Start with the identity matrix
        for n = 1:N
            M_total = M_period * M_total;  % Multiply N times
        end

        % Add the final layer if an odd number of layer pairs

        %M_total = M1 * M_total;

        % Include air and substrate
        if strcmpi(polarization, 's')
            % s-polarization (TE mode)
            I0 = [1, 1; n0 * cos(theta0), -n0 * cos(theta0)];
            Is = [1, 1; ns_idx * cos(theta_s), -ns_idx * cos(theta_s)];
        elseif strcmpi(polarization, 'p')
            % p-polarization (TM mode)
            I0 = [1, 1; n0 / cos(theta0), n0 / -cos(theta0)];
            Is = [1, 1; ns_idx / cos(theta_s), -ns_idx / cos(theta_s)];
        end
```

```
        % Total system matrix
        S = inv(I0) * M_total * inv(Is);

        % Extract reflection and transmission coefficients
        if strcmpi(polarization, 's')
            r = S(2, 1) / S(1, 1);
            t = 1 / S(1, 1);
        elseif strcmpi(polarization, 'p')
            r = S(2, 1) / S(1, 1);
            t = 1 / S(1, 1);
        end

        % Calculate reflectance and transmittance
        R(idx) = abs(r)^2;
        T(idx) = abs(t)^2 * (real(ns_idx * cos(theta_s)) / real(n0 * cos(theta0)));
    end
end
%https://www.degruyter.com/document/doi/10.1515/nanoph-2020-0212/html: A simple
transfer-matrix model for metasurface multilayer systems
%Annemarie Berkhout and A. Femius Koenderink
%"General transfer-matrix method for optical multilayer systems with coherent,
partially coherent, and incoherent interference
%Charalambos C. Katsidis and Dimitrios I. Siapkas" doi.org/10.1364/AO.41.003978
```